Regularization dependence on phase diagram in Nambu–Jona-Lasinio model

H. Kohyama [a], D. Kimura [b,*], T. Inagaki [c]

[a] *Department of Physics, National Taiwan University, Taipei 10617, Taiwan*
[b] *General Education, Ube National College of Technology, Ube, Yamaguchi 755-8555, Japan*
[c] *Information Media Center, Hiroshima University, Higashi-Hiroshima, Hiroshima 739-8521, Japan*

Abstract

We study the regularization dependence on meson properties and the phase diagram of quark matter by using the two flavor Nambu–Jona-Lasinio model. The model also has the parameter dependence in each regularization, so we explicitly give the model parameters for some sets of the input observables, then investigate its effect on the phase diagram. We find that the location or the existence of the critical end point highly depends on the regularization methods and the model parameters. Then we think that regularization and parameters are carefully considered when one investigates the QCD critical end point in the effective model studies.

1. Introduction

The phase structure of quark matter on finite temperature and density has actively been studied for decades [1]. Under usual condition, meaning low temperature and density, quarks are confined inside hadrons and they are never able to be observed as a single particle. On the other hand, due to the nature of the asymptotic freedom [2], quarks and gluons can be free from the confinement

at high temperature and density, because the coupling strength becomes weak at high energy. It is, therefore, expected that quark matter undergoes the confined/deconfined phase transition at some temperature and density. This is important subject both in theoretical and experimental studies since it crucially relates to the quark matter properties at relativistically high energy collisions and extremely dense stellar objects such as neutron stars.

The first principle for quarks and gluons is Quantum Chromodynamics (QCD) which is a non-Abelian gauge field theory for fermions. Our goal is to evaluate the phase structure based on this first principle QCD, however, it is difficult to extract theoretical predictions due to the nature of complicated strongly interacting system. One of the most reliable approaches is to use the discretized version of QCD called the Lattice QCD (LQCD) in which theoretical calculation is performed on the discrete spacetime [3]. Although the LQCD works well at finite temperature T for small chemical potential $\mu \simeq 0$, there is the technical difficulty called the "sign problem" when one tries to investigate the system at intermediate chemical potential. There effective models maybe nicely adopted because some models can consistently treat the system at finite temperature and chemical potential.

For the sake of evaluating the phase structure of quark matter at finite temperature and chemical potential, we will employ the Nambu–Jona-Lasinio (NJL) model [4] which is the most frequently used one in this context (there are a lot of nice review papers on the model, see, e.g. [5–9]). The model is constructed by incorporating the four point quark interaction into the model Lagrangian, so it is not renormalizable due to this higher dimensional operator. Therefore, the physical predictions of the model inevitably depend on the regularization procedure and the model parameters chosen. The resulting phase diagram on the $T-\mu$ plane is as well affected by the parameters and regularization prescriptions. So it is an important issue to study whether the phase structure obtained in one regularization method is consistent with the ones from different regularization methods.

The model parameters are fixed to reproduce some physical observables. Thus the model generally depends on the choice of the observables. We explicitly give the procedure to fix the model parameters and show the phase diagram for the following sets of inputs:

1. Pion mass, pion decay constant, and current quark mass,
2. Pion mass, pion decay constant, and constituent quark mass,
3. Pion mass, pion decay constant, and critical temperature at $\mu = 0$.

In this paper, we are going to study the phase structure of quark matter in the NJL model with various regularization ways, which are three dimensional (3D) momentum cutoff, four dimensional (4D) momentum cutoff, Pauli–Villars (PV) regularization, proper-time (PT) regularization, and the dimensional regularization (DR). The 3D cutoff scheme is the most popular method in this model and a lot of works have been done in this way. The 4D cutoff method preserves the Lorentz symmetry in which space and time are treated on equal footing. The Pauli–Villars regularization is based on the subtraction of the amplitude considering the virtually heavy particle to suppress the unphysical high energy contribution coming from loop integrals [10–12]. The proper-time regularization makes integrals finite through the exponentially dumping factor [11,13]. The dimensional regularization analytically continues the spacetime dimension in the loop integrals to a non-integer value, then try to obtain finite contribution from the integrals [14]. Beside from the frequently used 3D cutoff way, there have been a lot of works by using the 4D [6,7], PV [6,15–17], PT [6,18–26], and DR [27–32]. Thus, the physical consequences depend on the regularization [34]. It is also worth mentioning that regularization basically restricts

the region of the momentum integral or modifies the integrand to remove divergences coming from loop integrals, so it closely relates to the shape of the form factor [33].

This paper is organized as follows; Section 2 introduces the model Lagrangian, and shows the model treatment on the meson properties and the explicit formalism at finite temperature and chemical potential. In Section 3, we present various regularization procedures, 3D, 4D, PV, PT and DR prescriptions with explicit equations. We then perform the parameter fitting in Section 4. In Section 5, the numerical results of the meson properties are shown. We draw the phase diagrams with several parameter sets using various regularization methods in Section 6. We also study the phase diagram with the parameters fixed under the condition with the same constituent quark mass in Section 7, and the same critical temperature at $\mu = 0$ in Section 8. In Section 9, we give the discussions on the obtained results. Finally, we write the concluding remarks in Section 10. Several detailed calculations are shown in Appendices A and B.

2. Two flavor NJL model

In this paper we consider two light quarks with equal mass. The model has $SU_L(2) \otimes SU_R(2)$ flavor symmetry at the massless limit, $m \to 0$.

2.1. The Lagrangian and gap equation

The Lagrangian of the two flavor NJL model is given by

$$\mathcal{L} = \bar{\psi}(i\partial\!\!\!/ - \hat{m})\psi + G\left[(\bar{\psi}\psi)^2 + (\bar{\psi}i\gamma_5\tau^a\psi)^2\right], \tag{1}$$

where $\hat{m}$ is the diagonal mass matrix $\hat{m} = \mathrm{diag}(m_u, m_d)$ and G is the effective coupling strength of the four point interaction. We set $m_d = m_u$ in this paper. The application of the mean-field approximation

$$\langle \bar{\psi}\psi \rangle \simeq -\frac{\sigma}{2G} \tag{2}$$

leads the following mean-field Lagrangian

$$\tilde{\mathcal{L}} = \bar{\psi}(i\partial\!\!\!/ - m^*)\psi - \frac{\sigma^2}{4G}, \tag{3}$$

with the constituent mass $m^* = m_u + \sigma$. The flavor symmetry is broken down, $SU_L(2) \otimes SU_R(2) \to SU_{L+R}(2)$, by non-vanishing current quark mass, m_u, and dynamically generated σ. Thanks to the simple form of the Lagrangian, one can easily evaluate the effective potential, $\mathcal{V}_{\mathrm{eff}} = -\ln Z/V$ where Z is the partition function

$$Z = \int \mathcal{D}[\psi] \exp\left[i \int \mathrm{d}^4 x \, \tilde{\mathcal{L}}\right] \tag{4}$$

and V is the volume of the system. After some algebra, we see

$$\mathcal{V}_{\mathrm{eff}}(\sigma) = \frac{\sigma^2}{4G} - \int \frac{\mathrm{d}^4 k}{i(2\pi)^4} \ln \det(k\!\!\!/ - m^*). \tag{5}$$

The detailed derivation of the effective potential is presented in [9].

The gap equation is obtained through the extreme condition of the potential with respect to σ, namely,

$$\frac{\partial \mathcal{V}_{\text{eff}}}{\partial \sigma} = 0. \tag{6}$$

This condition leads the following gap equation

$$\sigma = 2N_f G \cdot i\text{tr}S(m^*), \tag{7}$$

with the number of flavors N_f and

$$i\text{tr}S(m^*) = -\text{tr} \int \frac{d^4k}{i(2\pi)^4} \frac{1}{\not{k} - m^* + i\varepsilon}, \tag{8}$$

where trace takes the spinor and color indices. This is the key equation in the model because it determines the values of the chiral condensate $\langle \overline{\psi}\psi \rangle$ and the constituent quark mass m^*.

2.2. Meson properties

The properties of the pion and sigma meson can be studied based on the model with the determined chiral condensate. The interacting Lagrangian of the pion and quarks is written by

$$\mathcal{L}_{\pi qq} = ig_{\pi qq}\overline{\psi}\gamma_5\tau \cdot \pi\psi, \tag{9}$$

where τ_i are 2×2 matrices in the flavor space and π^i represent the pion fields. The explicit expression is $\tau \cdot \pi = \tau_-\pi^- + \tau_+\pi^+ + \tau_0\pi^0$, with $\tau_\pm = (\tau_1 \pm \tau_2)/\sqrt{2}$ and $\tau_0 = \tau_3$ where τ_i are the Pauli matrices.

By applying the random phase approximation, we can write the pion propagator as the summation of the geometrical series of the one-loop diagram, which gives

$$\Delta_\pi(p^2) = \frac{g_{\pi qq}^2}{p^2 - m_\pi^2} \simeq \frac{2G}{1 - 2G\Pi^\pi(p^2)}, \tag{10}$$

where Π^π is the following quark loop contribution

$$\Pi^\pi(p^2) = -2 \int \frac{d^4k}{i(2\pi)^4}\text{tr}\left[\gamma_5 S(k)\gamma_5 S(k-p)\right], \tag{11}$$

with the quark propagator

$$S(k) = \frac{1}{\not{k} - m^* + i\epsilon}. \tag{12}$$

The explicit derivation of Eq. (10) is discussed in the review paper [6]. The pion mass is calculated at the pole position of the propagator, so the condition reads

$$\left[1 - 2G\Pi^\pi(p^2)\right]\big|_{p^2=m_\pi^2} = 0. \tag{13}$$

It should be noted that the residue at the pole $p^2 = m_\pi^2$ coincides with the square of the coupling strength $g_{\pi qq}^2$ so we have the relation

$$g_{\pi qq}^2 = \left(\frac{\partial \Pi^\pi}{\partial p^2}\right)^{-1}\Bigg|_{p^2=m_\pi^2}. \tag{14}$$

In the similar manner, the sigma meson mass is evaluated at the pole of the propagator,

$$\Delta_\sigma(p^2) = \frac{g_{\sigma qq}^2}{p^2 - m_\sigma^2} \simeq \frac{2G}{1 - 2G\Pi^\sigma(p^2)}, \tag{15}$$

with

$$\Pi^\sigma(p^2) = -2 \int \frac{d^4k}{i(2\pi)^4} \mathrm{tr}\left[S(k)S(k-p)\right]. \tag{16}$$

Therefore the condition which determines the sigma meson mass becomes

$$\left[1 - 2G\Pi^\sigma(p^2)\right]\big|_{p^2=m_\sigma^2} = 0. \tag{17}$$

The pion decay constant is calculated from the following equation

$$i\delta_{ij}p^\mu f_\pi = \langle 0|\bar\psi \frac{\tau_j}{2}\gamma^\mu \gamma_5 \psi|\pi_i\rangle. \tag{18}$$

The explicit form becomes

$$p^\mu f_\pi = \frac{1}{2} \int \frac{d^4k}{i(2\pi)^4} \mathrm{tr}\left[\gamma^\mu \gamma_5 g_{\pi qq} S(k)\gamma_5 S(k-p)\right]. \tag{19}$$

Thus Eqs. (13), (17) and (19) are the ones which determine the pion mass, sigma meson mass, and the pion decay constant.

2.3. Explicit formalism at finite temperature

Since our purpose is to study the phase structure on temperature T and chemical potential μ, we need to extend the equations to the formulae with finite temperature and chemical potential. According to the imaginary time formalism, the integral region of the temporal component becomes finite due to the periodic or anti-periodic condition of fields as

$$Z = \int \mathcal{D}[\psi] \exp\left[\int_0^\beta d\tau \int d^3\mathbf{x}\left(\tilde{\mathcal{L}} + \mu\bar\psi \gamma_0 \psi\right)\right], \tag{20}$$

where τ is imaginary time and β is the inverse temperature $1/T$. Consequently, continuous integral in the temporal direction is replaced by the following discrete summation,

$$\int \frac{d^4k}{i(2\pi)^4} F(k_0, \mathbf{k}) \rightarrow T \sum_{n=-\infty}^{\infty} \int \frac{d^3k}{(2\pi)^3} F(i\omega_n + \mu, \mathbf{k}), \tag{21}$$

where $\omega_n = 2n\pi T$ or $(2n+1)\pi T$ depending on the statistical property of field, i.e., for bosons or fermions, and the chemical potential seen in Eq. (20) appears in the way $i\omega_n + \mu$. In this paper, we only treat fermionic quark loop contributions then $\omega_n = (2n+1)\pi T$ is always the case.

With the help of the formalism Eq. (21), we see that the gap equation at finite temperature becomes

$$\sigma = 2N_f G \cdot [\mathrm{tr}S^0 + \mathrm{tr}S^T], \tag{22}$$

$$\mathrm{tr}S^0 = -N_c m^* \int \frac{d^3k}{(2\pi)^3} \frac{1}{2E}, \tag{23}$$

$$\mathrm{tr}S^T = N_c m^* \int \frac{d^3k}{(2\pi)^3} \frac{1}{2E}\left[\sum_\pm f(E^\pm)\right], \tag{24}$$

where N_c is the number of colors, $E = \sqrt{k^2 + m^{*2}}$, $E^{\pm} = E \pm \mu$ and $f(E) = 1/(1 + e^{\beta E})$. It is important to note that the contributions can be expressed by the summation of the T independent part ($\mathrm{tr}S^0$) and T dependent part ($\mathrm{tr}S^T$). This characteristic is general if one takes the infinite number of the frequency summation in finite temperature field theory and crucial when we apply the regularization procedures to the appearing integrals.

Since the gap equation is derived by differentiating the effective potential with respect to σ, then the effective potential can be obtained by integrating the gap equation (see, for example, [36]),

$$\mathcal{V}(\sigma) = \frac{\sigma^2}{4G} - N_f \int\limits_0^\sigma \mathrm{d}\sigma' \, i\mathrm{tr}S(m_u + \sigma'), \tag{25}$$

where we have dropped the suffix in $\mathcal{V}_{\mathrm{eff}}$ and just written $\mathcal{V}$ for notational simplicity. Thereafter the effective potential at finite temperature $\mathcal{V} = \mathcal{V}^\sigma + \mathcal{V}^0 + \mathcal{V}^T$ is evaluated as

$$\mathcal{V}^\sigma = \frac{\sigma^2}{4G}, \tag{26}$$

$$\mathcal{V}^0 = -2N_f N_c \int \frac{\mathrm{d}^3 k}{(2\pi)^3} E, \tag{27}$$

$$\mathcal{V}^T = -2N_f N_c T \int \frac{\mathrm{d}^3 k}{(2\pi)^3} \sum_\pm \ln\left[1 + e^{-\beta E^\pm}\right]. \tag{28}$$

It is important to note that, if we apply some regularizations, the results between the direct calculation from Eq. (5) and the one after integrating the gap equation may become different, because regularization essentially means the subtraction and there are several ways of subtractions. Therefore, in this paper, we persistently use the latter way shown in Eq. (25) so that the model treatment becomes consistent. It should be noticed that the finite temperature correction, $\mathcal{V}^T$, contains no divergent integral. A finite result can be obtained for the finite temperature correction without applying any regularizations.

Next, we carry on the integral in the meson properties; the one loop contribution can be written as

$$\Pi^\pi(p^2) = -\frac{2\mathrm{tr}S}{m^*} + p^2 I(p^2), \tag{29}$$

with

$$I(p^2) = 4N_c \int \frac{\mathrm{d}^4 k}{i(2\pi)^4} \frac{1}{(k^2 - m^{*2})[(k-p)^2 - m^{*2}]}. \tag{30}$$

Since $\mathrm{tr}S$ is already evaluated above, the remaining task is to calculate $I(= I^0 + I^T)$, and it becomes

$$I^0(p^2) = 4N_c \int \frac{\mathrm{d}^3 k}{(2\pi)^3} \frac{1}{E(4E^2 - p^2)}, \tag{31}$$

$$I^T(p^2) = -4N_c \int \frac{\mathrm{d}^3 k}{(2\pi)^3} \frac{\sum_\pm f(E^\pm)}{E(4E^2 - p^2)}. \tag{32}$$

Similarly, the one-loop diagram of the scalar channel can be written as

$$\Pi^\sigma(p^2) = -\frac{2\mathrm{tr}S}{m^*} + (p^2 - 4m^{*2})\, I(p^2). \tag{33}$$

We now have already evaluated all the ingredients of Π^σ above in Eqs. (23), (24), (31) and (32), so we do not need further calculations.

Finally, let us derive the equation for the pion decay constant. After a bit of algebra we obtain the relation,

$$f_\pi = g_{\pi qq} m^* I(0). \tag{34}$$

Here we evaluate f_π at $p^2 = 0$ following [6].

3. Regularization procedures

Since the integrals obtained in the previous section include infinities, we need to apply some regularization so that the model leads finite quantities. As mentioned in the introduction, the model is not renormalizable, then the model predictions inevitably depend on regularization procedures chosen. Here, we shall present possible regularization methods in this section.

3.1. Three dimensional cutoff scheme

The idea of the three dimensional (3D) cutoff is simple; one drops high frequency mode by introducing the cutoff scale Λ_{3D} into the integrals. We work in the 3-dimensional polar coordinate system and cut the radial coordinate as

$$\int \frac{\mathrm{d}^4 k}{(2\pi)^4} \rightarrow \int \frac{\mathrm{d}k_0}{2\pi} \int_0^{\Lambda_{3D}} \frac{k^2 \mathrm{d}k}{(2\pi)^3} \int d\Omega_3. \tag{35}$$

By performing the integrals, we have for the gap equation $\sigma = 2N_f G\, \mathrm{tr}S$,

$$\mathrm{tr}S_{3D}^0 = \frac{N_c m^*}{2\pi^2} \left(\Lambda_{3D}\sqrt{\Lambda_{3D}^2 + m^{*2}} - m^{*2} \ln \frac{\Lambda_{3D} + \sqrt{\Lambda_{3D}^2 + m^{*2}}}{m^*} \right), \tag{36}$$

$$\mathrm{tr}S_{3D}^T = -\frac{N_c m^*}{\pi^2} \int_0^{\Lambda_{3D}} \mathrm{d}k \, \frac{k^2}{E} \left[\sum_{\pm} f(E^\pm) \right]. \tag{37}$$

The effective potential can also be calculated as

$$\mathcal{V}_{3D}^0(\sigma) = -\frac{N_c N_f}{8\pi^2} \left[\Lambda_{3D}\sqrt{\Lambda_{3D}^2 + m^{*2}}(2\Lambda_{3D}^2 + m^{*2}) - m^{*4} \ln \frac{\Lambda_{3D}\sqrt{\Lambda_{3D}^2 + m^{*2}}}{m^*} \right], \tag{38}$$

$$\mathcal{V}_{3D}^T(\sigma) = -\frac{N_c N_f T}{\pi^2} \int_0^{\Lambda_{3D}} \mathrm{d}k \, k^2 \left[\sum_{\pm} \ln(1 + e^{-\beta E^\pm}) \right]. \tag{39}$$

The quark loop integral in the meson properties $I(p^2)$ reads

$$I^0_{3D} = \frac{2N_c}{\pi^2} \int\limits_0^{\Lambda_{3D}} dk \, \frac{k^2}{E(4E^2 - p^2)}, \tag{40}$$

$$I^T_{3D} = -\frac{2N_c}{\pi^2} \int\limits_0^{\Lambda_{3D}} dk \, \frac{k^2}{E(4E^2 - p^2)} \left[\sum_{\pm} f(E^{\pm}) \right]. \tag{41}$$

Note that the integral diverges around $4E^2 \simeq p^2$, and we apply the principal integral to avoid this divergence [35]. It may be worth mentioning that the integral can be performed analytically when $p^2 = 0$ for $T = 0$, then one has for the pion decay constant,

$$f^2_{\pi 3D} = \frac{N_c m^{*2}}{2\pi^2} \left(-\frac{\Lambda_{3D}}{\sqrt{\Lambda^2_{3D} + m^{*2}}} + \ln \frac{\Lambda_{3D} + \sqrt{\Lambda^2_{3D} + m^{*2}}}{m^*} \right). \tag{42}$$

We thus obtain the required quantities in evaluating the phase diagram and meson properties.

3.2. Four dimensional cutoff scheme

In the four dimensional (4D) cutoff regularization scheme, we introduce the cutoff scale Λ_{4D} in the Euclidean space after performing the Wick rotation,

$$\int \frac{d^4 k_E}{(2\pi)^4} \rightarrow \int\limits_0^{\Lambda_{4D}} \frac{k_E^3 dk_E}{(2\pi)^4} \int d\Omega_4. \tag{43}$$

This is well known four dimensional cutoff method for $T = 0$ case. As the natural extension to finite temperature, we introduce the cutoff scale by

$$\int \frac{d^4 k_E}{(2\pi)^4} \rightarrow T \sum_{n=-L_4-1}^{L_4} \int\limits_0^{\sqrt{\Lambda^2_{4D} - \omega_n^2}} \frac{k^2 dk}{(2\pi)^3} \int d\Omega_3, \tag{44}$$

where L_4 is the maximum integer which does not exceed $\Lambda_{4D}/(2\pi T) - 1/2$.

In the 4D cutoff way, it is difficult to divide the contribution into the temperature independent and dependent parts, since there is also cutoff in the frequency summation.

The explicit form of $\mathrm{tr}S$ and the effective potential become

$$\mathrm{tr}S_{4D} = \frac{N_c m^* T}{2\pi^2} \sum_{n=-L_4-1}^{L_4} \int\limits_0^{\sqrt{\Lambda^2_{4D} - \omega_n^2}} dk k^2 \frac{1}{(\omega_n^-)^2 + E^2}, \tag{45}$$

$$\mathcal{V}_{4D}(\sigma) = -\frac{N_c N_f T}{4\pi^2} \sum_{n=-L_4-1}^{L_4} \int\limits_0^{\sqrt{\Lambda^2_{4D} - \omega_n^2}} dk k^2 \ln((\omega_n^-)^2 + E^2), \tag{46}$$

where $\omega_n^- = \omega_n - i\mu$.

For $T = 0$, the integral can be performed analytically by using the Feynman parameter method,

$$\text{tr}S_{4D}^0 = \frac{N_c m^*}{\pi^2}\left[\Lambda_{4D}^2 - m^{*2}\ln\left(\frac{\Lambda_{4D}^2 + m^{*2}}{m^{*2}}\right)\right], \tag{47}$$

$$\mathcal{V}_{4D}^0(\sigma) = -\frac{N_c N_f}{8\pi^2}\left[\Lambda_{4D}^2 m^{*2} - m^{*4}\ln\frac{\Lambda_{4D}^2 + m^{*2}}{m^{*2}} + \Lambda_{4D}^{*4}\ln(\Lambda_{4D}^2 + m^{*2})\right]. \tag{48}$$

One should give the special attention in calculating $I_{4D}(p^2)$, because the integral includes divergence to be cured as seen in the 3D cutoff case. The analytic expression of $I_{4D}^0(p^2)$ will be given in Appendix A.

Again we show the explicit form for the pion decay constant at $T = 0$,

$$f_{\pi 4D}^2 = \frac{N_c m^{*2}}{4\pi^2}\left[-\frac{\Lambda_{4D}^2}{\Lambda_{4D}^2 + m^{*2}} + \ln\left(\frac{\Lambda_{4D}^2 + m^{*2}}{m^{*2}}\right)\right]. \tag{49}$$

3.3. Pauli–Villars regularization

In this regularization, the divergences from loop integrals are subtracted by introducing virtually heavy particles as

$$\frac{1}{k^2 - m^2} \longrightarrow \frac{1}{k^2 - m^2} - \sum_i \frac{a_i}{k^2 - \Lambda_i^2}. \tag{50}$$

This manipulation induces virtual frictional force so that the contribution from unphysical high frequency mode is suppressed.

In evaluating the gap equation, we apply the following subtraction

$$\frac{1}{p^2 - m^{*2}} - \frac{a_1}{p^2 - \Lambda_1^2} - \frac{a_2}{p^2 - \Lambda_2^2}, \tag{51}$$

where

$$a_1 = \frac{m^{*2} - \Lambda_2^2}{\Lambda_1^2 - \Lambda_2^2}, \quad a_2 = \frac{\Lambda_1^2 - m^{*2}}{\Lambda_1^2 - \Lambda_2^2}. \tag{52}$$

By setting the cutoff scales $\Lambda_1 = \Lambda_2 = \Lambda_{PV}$ after the subtraction, we have

$$\text{tr}S_{PV}^0 = \frac{N_c m^*}{4\pi^2}\left(\Lambda_{PV}^2 - m^{*2} + m^{*2}\ln\frac{m^{*2}}{\Lambda_{PV}^{*2}}\right), \tag{53}$$

$$\text{tr}S_{PV}^T = -2N_c m^*\int\frac{d^3 p}{(2\pi)^3}\left[\frac{f(E_m^\pm)}{E_m} - \left(1 + \frac{\Lambda_{PV}^2 - m^{*2}}{2p^2}\right)\frac{f(E_\Lambda^\pm)}{E_\Lambda}\right], \tag{54}$$

where $E_m = \sqrt{k^2 + m^{*2}}$ and $E_\Lambda = \sqrt{k^2 + \Lambda_{PV}^2}$. By integrating the above equation, we obtain the effective potential

$$
\mathcal{V}_{\mathrm{PV}}^0 = -\frac{N_c N_f}{8\pi^2}\left[\Lambda_{\mathrm{PV}}^2 m^{*2} - \frac{3}{4}m^{*4} + \frac{1}{2}m^{*4}\ln\frac{m^{*2}}{\Lambda_{\mathrm{PV}}^2}\right],
\tag{55}
$$

$$
\mathcal{V}_{\mathrm{PV}}^T = -\frac{N_c N_f T}{\pi^2}\sum_{\pm}\int \mathrm{d}k\left[k^2\ln(1+e^{-\beta E_m^\pm}) - \frac{m^2}{8}(4k^2+2\Lambda^2-m^{*2})\frac{f(E_\Lambda^\pm)}{E_\Lambda}\right].
\tag{56}
$$

Since the divergence coming from the integral $I(p^2)$ is order of log, one subtraction is enough to make it finite, so we get

$$
I_{\mathrm{PV}}^0 = \frac{2N_c}{\pi^2}\int \mathrm{d}kk^2\left[\frac{1}{E_m(4E_m^2-p^2)} - \frac{1}{E_\Lambda(4E_\Lambda^2-p^2)}\right],
\tag{57}
$$

$$
I_{\mathrm{PV}}^T = -\frac{2N_c}{\pi^2}\int \mathrm{d}kk^2\left[\frac{\sum_\pm f(E_m^\pm)}{E_m(4E_m^2-p^2)} - \frac{\sum_\pm f(E_\Lambda^\pm)}{E_\Lambda(4E_\Lambda^2-p^2)}\right].
\tag{58}
$$

The pion decay constant at $T=0$ becomes

$$
f_{\pi\mathrm{PV}}^2 = \frac{N_c m^{*2}}{4\pi^2}\left(-1+\frac{\Lambda_{\mathrm{PV}}^2}{\Lambda_{\mathrm{PV}}^2-m^{*2}}\ln\frac{\Lambda_{\mathrm{PV}}^2}{m^{*2}}\right).
\tag{59}
$$

3.4. Proper-time regularization

The basic idea of the proper-time regularization is based on the following manipulation of the Gamma function,

$$
\frac{1}{A^n} \to \frac{1}{\Gamma[n]}\int\limits_{1/\Lambda_{\mathrm{PT}}^2}^{\infty}\mathrm{d}\tau\,\tau^{n-1}e^{-A\tau},
\tag{60}
$$

where the lower cut $1/\Lambda_{\mathrm{PT}}^2$ induces the dumping factor into the original propagator, for example with $n=1$,

$$
\frac{1}{k_E^2+m^{*2}} \to \int\limits_{1/\Lambda_{\mathrm{PT}}^2}^{\infty}\mathrm{d}\tau\,e^{-A\tau} = \frac{1}{k_E^2+m^{*2}}e^{-(k_E^2+m^{*2})/\Lambda_{\mathrm{PT}}^2}.
\tag{61}
$$

Therefore in this regularization high frequency contribution is dumped by the factor $e^{-k_E^2/\Lambda_{\mathrm{PT}}^2}$, so the original divergent integral turns out to be finite. For A which contains an imaginary part, Eq. (60) is modified as,

$$
\frac{1}{A^n} \to \frac{i^n}{\Gamma[n]}\int\limits_{+0}^{\infty}\mathrm{d}\tau\,\tau^{n-1}e^{-iA\tau}, \quad (\mathrm{Im}(A)<0,\ \mathrm{Re}(n)>0).
\tag{62}
$$

Under this procedure, the integral of $\mathrm{tr}S$ in the gap equation becomes

$$
\mathrm{tr}S_{\mathrm{PT}}^0 = \frac{N_c m^*}{4\pi^2}\left[\Lambda_{\mathrm{PT}}^2 e^{-m^{*2}/\Lambda_{\mathrm{PT}}^2} + m^{*2}Ei(-m^{*2}/\Lambda_{\mathrm{PT}}^2)\right],
\tag{63}
$$

$$
\mathrm{tr}S_{\mathrm{PT}} = \frac{N_c m^* T}{2\pi^{3/2}}\sum_{n=0}^{\infty}\int\limits_{+0}^{\infty}\frac{\mathrm{d}\tau}{\tau^{3/2}}\left[e^{-i\pi/4}e^{-i\{(\omega_n^-)^2+m^{*2}\}\tau} + c.c.\right],
\tag{64}
$$

where $Ei(-x)$ is the exponential-integral function. For $m^{*2} \ll \Lambda_{\text{PT}}^2$, Eq. (63) is expanded as

$$\text{tr} S_{\text{PT}}^0 \simeq \frac{N_c m^*}{4\pi^2} \left[\Lambda_{\text{PT}}^2 - m^{*2} + m^{*2} \left(\ln \frac{m^{*2}}{\Lambda_{\text{PT}}^2} + \gamma_E - \frac{m^{*2}}{2\Lambda_{\text{PT}}^2} \right) \right]. \tag{65}$$

We rotate the contour of the integration in Eq. (64) to the imaginary axis of τ [23–25]. For $\omega_0^2 - \mu^2 + m^{*2} > 0$, the trace becomes

$$\text{tr} S_{\text{PT}} = \frac{N_c m^* T}{\pi^{3/2}} \sum_{n=0}^{\infty} \int_{1/\Lambda_{\text{PT}}^2}^{\infty} \frac{d\tau}{\tau^{3/2}} \cos(2\omega_n \mu \tau) e^{-(\omega_n^2 - \mu^2 + m^{*2})\tau}, \tag{66}$$

and for $\omega_0^2 - \mu^2 + m^{*2} < 0$,

$$\text{tr} S_{\text{PT}} = \frac{N_c m^* T}{\pi^{3/2}} \left[\sum_{n>[N]}^{\infty} \int_{1/\Lambda_{\text{PT}}^2}^{\infty} \frac{d\tau}{\tau^{3/2}} \cos(2\omega_n \mu \tau) e^{-(\omega_n^2 - \mu^2 + m^{*2})\tau} \right.$$

$$- \sum_{n=0}^{[N]} \left\{ \int_{1/\Lambda_{\text{PT}}^2}^{\infty} \frac{d\tau}{\tau^{3/2}} \sin(2\omega_n \mu \tau) e^{(\omega_n^2 - \mu^2 + m^{*2})\tau} \right.$$

$$\left. \left. - \Lambda_{\text{PT}} \, \text{Re} \left(e^{i\pi/4} \int_{-\pi/2}^{\pi/2} d\theta \, e^{-i\theta/2} \exp\left[-i\{(\omega_n^-)^2 + m^{*2}\} e^{i\theta} / \Lambda_{\text{PT}}^2 \right] \right) \right\} \right], \tag{67}$$

where $N = \{\sqrt{\mu^2 - m^{*2}}/(\pi T) - 1\}/2$. Similarly, the effective potential can be calculated through

$$\mathcal{V}_{\text{PT}}(\sigma) = \frac{N_c N_f T}{4\pi^{3/2}} \sum_{n=0}^{\infty} \int_{+0}^{\infty} \frac{d\tau}{\tau^{5/2}} \left[e^{-3i\pi/4} e^{-i\{(\omega_n^-)^2 + m^{*2}\}\tau} + c.c. \right]. \tag{68}$$

For $\omega_0^2 - \mu^2 + m^{*2} > 0$, one has

$$\mathcal{V}_{\text{PT}}(\sigma) = \frac{N_c N_f T}{2\pi^{3/2}} \sum_{n=0}^{\infty} \int_{1/\Lambda_{\text{PT}}^2}^{\infty} \frac{d\tau}{\tau^{5/2}} \cos(2\omega_n \mu \tau) e^{-(\omega_n^2 - \mu^2 + m^{*2})\tau}, \tag{69}$$

and for $\omega_0^2 - \mu^2 + m^{*2} < 0$,

$$\mathcal{V}_{\text{PT}}(\sigma) = \frac{N_c N_f T}{2\pi^{3/2}} \left[\sum_{n>[N]}^{\infty} \int_{1/\Lambda_{\text{PT}}^2}^{\infty} \frac{d\tau}{\tau^{5/2}} \cos(2\omega_n \mu \tau) e^{-(\omega_n^2 - \mu^2 + m^{*2})\tau} \right.$$

$$+ \sum_{n=0}^{[N]} \left\{ \int_{1/\Lambda_{\text{PT}}^2}^{\infty} \frac{d\tau}{\tau^{5/2}} \sin(2\omega_n \mu \tau) e^{(\omega_n^2 - \mu^2 + m^{*2})\tau} \right.$$

$$+ \Lambda^3 \, \mathrm{Re}\!\left(e^{-i\pi/4} \int_{-\pi/2}^{\pi/2} d\theta \, e^{-3i\theta/2} \exp\left[-i\{(\omega_n^-)^2 + m^{*2}\}e^{i\theta}/\Lambda_{\mathrm{PT}}^2\right]\right)\Bigg\}\Bigg]. \qquad (70)$$

I_{PT} can also be calculated by

$$I_{\mathrm{PT}}(p^2) = -\frac{N_c T}{\pi^{3/2}} \sum_{n=0}^{\infty} \int_0^{1/2} d\alpha \int_{+0}^{\infty} \frac{d\tau}{\tau^{1/2}} \left[e^{-3i\pi/4} e^{-i\{(\omega_n^-)^2 + \Delta\}\tau} + c.c.\right], \qquad (71)$$

where α is the Feynman integration parameter and $\Delta = m^{*2} - p^2/4 + \alpha^2 p^2$. Then the integral can be written

$$I_{\mathrm{PT}}(p^2) = \frac{2N_c T}{\pi^{3/2}} \int_0^{1/2} d\alpha \sum_{n=0}^{\infty} \Bigg[\theta(W_n(\alpha)) \int_{1/\Lambda_{\mathrm{PT}}^2}^{\infty} \frac{d\tau}{\tau^{1/2}} \cos(2\omega_n \mu \tau) e^{-(\omega_n^2 - \mu^2 + \Delta)\tau}$$

$$+ \theta(-W_n(\alpha))\Bigg\{ \int_{1/\Lambda_{\mathrm{PT}}^2}^{\infty} \frac{d\tau}{\tau^{1/2}} \sin(2\omega_n \mu \tau) e^{(\omega_n^2 - \mu^2 + \Delta)\tau}$$

$$- \frac{1}{\Lambda} \, \mathrm{Re}\!\left(e^{-i\pi/4} \int_{-\pi/2}^{\pi/2} d\theta \, e^{i\theta/2} \exp\left[-i\{(\omega_n^-)^2 + \Delta\}e^{i\theta}/\Lambda_{\mathrm{PT}}^2\right]\right)\Bigg\}\Bigg], \qquad (72)$$

where $W_n(\alpha) = \omega_n^2 + m^{*2} + (\alpha^2 - 1/4)p^2 - \mu^2$.

The pion decay constant at $T = 0$ reads the following simple form,

$$f_{\pi \mathrm{PT}}^2 = -\frac{N_c m^{*2}}{4\pi^2} Ei(-m^{*2}/\Lambda_{\mathrm{PT}}^2). \qquad (73)$$

For $m^{*2} \ll \Lambda_{\mathrm{PT}}^2$, we have

$$f_{\pi \mathrm{PT}}^2 \simeq \frac{N_c m^{*2}}{4\pi^2} \left\{ -\gamma_E + \frac{m^{*2}}{\Lambda_{\mathrm{PT}}^2} + \ln\frac{\Lambda_{\mathrm{PT}}^2}{m^{*2}} \right\}. \qquad (74)$$

3.5. Dimensional regularization

In the dimensional regularization method, we obtain finite quantities through analytically continuing the dimension in the loop integral to a non-integer value, D, as

$$\int \frac{\mathrm{d}^4 k}{(2\pi)^4} \to M_0^{4-D} \int \frac{\mathrm{d}^D k}{(2\pi)^D}, \qquad (75)$$

where the scale parameter M_0 is inserted so as to adjust the mass dimension of physical quantities. The method is well known since it preserves most of symmetries. Note that this result is the same as the result obtained from the proper-time integral ($0 < \tau < \infty$) and expressed by the poles of the Gamma function.

The trace $\mathrm{tr}S$ in the gap equation reads

$$\mathrm{tr}S^0_{\mathrm{DR}} = \frac{-N_c M_0^{4-D} m^*}{(2\pi)^{D/2}} \Gamma\left(1 - \frac{D}{2}\right)(m^{*2})^{D/2-1}, \tag{76}$$

$$\mathrm{tr}S^T_{\mathrm{DR}} = -A_D m^* \int \mathrm{d}k \frac{k^{D-2}}{2E}\left[\sum_{\pm} f(E^\pm)\right], \tag{77}$$

where

$$A_D = \frac{N_c 2^{2-D/2} M_0^{4-D}}{\pi^{(D-1)/2} \Gamma((D-1)/2)}. \tag{78}$$

The effective potential becomes

$$\mathcal{V}^0_{\mathrm{DR}} = \frac{N_c N_f M_0^{4-D}}{2(2\pi)^{D/2}} \Gamma\left(-\frac{D}{2}\right)(m^{*2})^{D/2}, \tag{79}$$

$$\mathcal{V}^T_{\mathrm{DR}} = -A_D N_f T \int \mathrm{d}k\, k^{D-2} \sum_{\pm} \ln\left[1 + e^{-\beta E^\pm}\right]. \tag{80}$$

In the similar manner, the integral $I(p^2)$ appearing in the meson propagator is calculated as

$$I^0_{\mathrm{DR}} = A_D \int \mathrm{d}k \frac{k^{D-2}}{E(4E^2 - p^2)}, \tag{81}$$

$$I^T_{\mathrm{DR}} = A_D \int \mathrm{d}k \frac{-k^{D-2}}{E(4E^2 - p^2)}\left[\sum_{\pm} f(E^\pm)\right]. \tag{82}$$

Note we need to perform the principal integration for $m^{*2} < p^2/4$.

The pion decay constant at $T = 0$ reads the following simple form,

$$f^2_{\pi\mathrm{DR}} = \frac{N_c M_0^{4-D}}{(2\pi)^{D/2}} \Gamma\left(2 - \frac{D}{2}\right)(m^{*2})^{D/2-1}. \tag{83}$$

We show the concrete examples of $\mathrm{tr}S^0_{\mathrm{DR}}$ and $f^2_{\pi\mathrm{DR}}$ for $D \simeq 2, 3, 4$ in Appendix B.

4. Model parameters

Having obtained the equations which determine the pion mass and pion decay constant, we are now ready to perform the parameter fitting. In the previous section we suppose that all the cutoff scales are equal in each regularization to reduce the parameters. Thus the model has three parameters: the cutoff scale Λ, the current quark mass m_u and the coupling strength G. Whereas in the DR there appears one more parameter, so the total number becomes four: the current mass m_u, dimension D, scale parameter M_0 and the coupling G, as discussed in Ref. [37]. In this section, we shall set the model parameters by fitting the pion mass and decay constant. The actual values we use are shown below

$$m_\pi = 135\ \mathrm{MeV}, \quad f_\pi = 94\ \mathrm{MeV}. \tag{84}$$

Here we do not use the sigma meson mass and the decay width, because these values have large uncertainty, $m_\sigma = 400\text{–}550\ \mathrm{MeV}$ and $\Gamma_\sigma = 400\text{–}700\ \mathrm{MeV}$ [38]. The theoretical uncertainty is

Table 1
Parameters in the 3D cutoff.

m_u (MeV)	Λ_{3D} (MeV)	G (MeV^{-2})	m^* (MeV)	$\langle \bar{u}u \rangle^{1/3}$ (MeV)
3.0	942	2.00×10^{-6}	220	-300
4.0	781	3.09×10^{-6}	255	-272
5.0	665	4.71×10^{-6}	311	-253
5.5	609	6.26×10^{-6}	375	-245

Table 2
Parameters in the 4D cutoff.

m_u (MeV)	Λ_{4D} (MeV)	G (MeV^{-2})	m^* (MeV)	$\langle \bar{u}u \rangle^{1/3}$ (MeV)
3.0	1397	1.80×10^{-6}	198	-300
5.0	1027	3.64×10^{-6}	242	-253
8.0	768	8.88×10^{-6}	369	-216

Table 3
Parameters in the Pauli–Villars regularization.

m_u (MeV)	Λ_{PV} (MeV)	G (MeV^{-2})	m^* (MeV)	$\langle \bar{u}u \rangle^{1/3}$ (MeV)
3.0	1420	1.77×10^{-6}	195	-300
5.0	1071	3.45×10^{-6}	229	-253
8.0	853	6.78×10^{-6}	283	-216
10.0	778	9.64×10^{-6}	312	-198
15.0	729	19.4×10^{-6}	417	-173

Table 4
Parameters in the proper-time regularization.

m_u (MeV)	Λ_{PT} (MeV)	G (MeV^{-2})	m^* (MeV)	$\langle \bar{u}u \rangle^{1/3}$ (MeV)
3.0	1464	1.61×10^{-6}	178	-300
5.0	1097	3.07×10^{-6}	204	-253
8.0	849	5.85×10^{-6}	245	-216
10.0	755	8.13×10^{-6}	265	-198
15.0	645	17.2×10^{-6}	372	-173

also large. The sigma meson decays into an unphysical decay mode, a quark–antiquark pair, in the NJL model. It is a well-known problem which reflects the lack of confinement of the model. Note that the higher order corrections coming from the $\pi\pi$ scattering are essential for the sigma width [39,40]. To discuss the sigma meson width one should calculate the next to leading order corrections in the $1/N_c$ expansion. For the case with the DR, we perform fitting with one more quantity, the neutral pion decay width to two photons, which will be discussed later.

4.1. Parameters in various regularizations

Here we align the model parameters in various regularizations in this subsection.

Tables 1, 2, 3 and 4 show how the parameters change according to the current quark mass m_u, where we first set the value of m_u then search the parameters Λ and G which lead
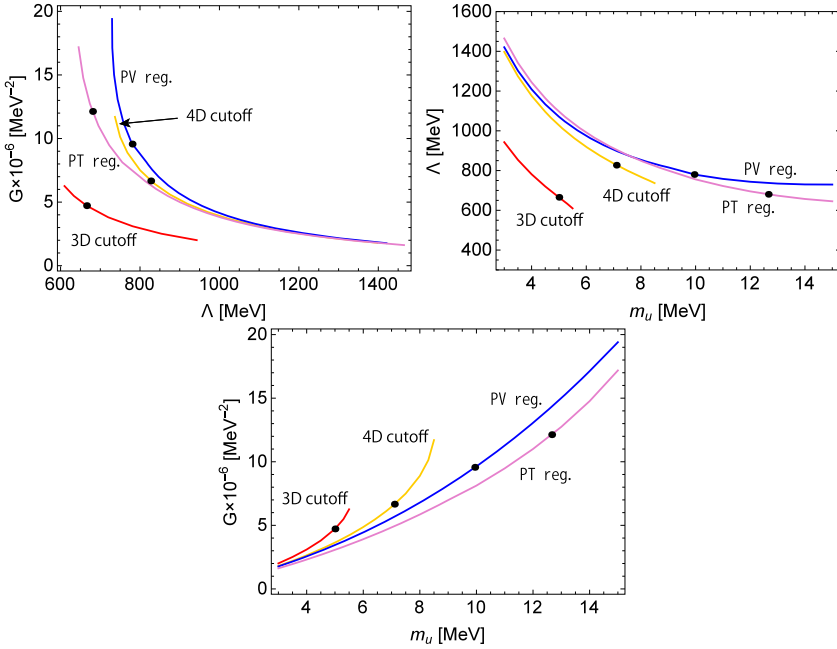
Fig. 1. Parameters in each regularization.

$m_\pi = 135$ MeV and $f_\pi = 94$ MeV. One sees the tendency that cutoff scale Λ becomes smaller with increasing m_u, while G becomes larger according to m_u. We confirm that the values of the cutoff and four point coupling are $O(10^3)$ and $O(10^{-6})$ in MeV scale in these regularizations.

We also showed the values of the constituent quark mass m^* and the chiral condensate $\langle \bar{u}u \rangle^{1/3}$ which are the predicted quantities in the models. We note that the values of m^* are about 200–400 MeV which are comparable to one third of the proton mass. We also note that m^* increases with respect to m_u, while the absolute value of $\langle \bar{u}u \rangle$ decreases when m_u becomes large. Since the relation $m^* \propto G\langle \bar{u}u \rangle$ holds, even $\langle \bar{u}u \rangle$ becomes smaller m^* can be larger due to the large value of G, which is actually the case in these regularizations. It should be noted that the values, $\langle \bar{u}u \rangle$, coincide under each regularization with fixed m_u. This regularization independent relation is deduced from the Gell-Mann–Oakes–Renner relation [42], $f_\pi^2 m_\pi^2 \simeq \sigma m_u/(2G)$, and the gap equation (7),

$$\langle \bar{u}u \rangle \simeq -\frac{f_\pi^2 m_\pi^2}{2m_u}. \tag{85}$$

We plot the parameters of each regularization in Fig. 1. The black circles denote the value which satisfy $m^* = 311$ MeV for each regularization. The relation between the cutoff scale Λ and G for the 4D cutoff, Pauli–Villars regularization and proper-time regularization resembles each other. The relation between m_u and Λ for these regularizations also resembles each other. In the case of same value for m^*, the m_u dependence of Λ is large. However, the values of Λ are close, 660–830 MeV. In the case of same value for m^*, the m_u dependence of G is large and the values of G are separate in each regularization. The relation between m_u and G is different in each regularization.

Table 5
Parameters in the dimensional regularization.

m_u (MeV)	D	GM_0^{4-D} (MeV^{-2})	M_0 (MeV)	m^* (MeV)	$\langle \bar{u}u \rangle^{1/3}$ (MeV)
3.0	2.37	-113.4×10^{-4}	110	-570	-299
4.0	2.47	-81.9×10^{-4}	104	-543	-272
5.0	2.56	-58.8×10^{-4}	97	-519	-253
8.0	2.78	-24.1×10^{-4}	80	-459	-217

4.2. Parameter fitting in the dimensional regularization

For the sake of the parameter fitting in the DR, we present the calculation of the decay width for the pion to two photon decays, $\Gamma_{\pi^0 \gamma\gamma}$, in this subsection. The decay width can be evaluated through the following one-loop amplitude, $T_{\mu\nu}(k_1, k_2)$,

$$T_{\mu\nu}(k_1, k_2) = 4i\epsilon_{\mu\nu\rho\lambda} k_1^\rho k_2^\lambda \cdot T_\gamma, \tag{86}$$

$$T_\gamma = g_{\pi qq} e^2 \frac{N_c}{3} m^* M_0^{4-D} \int \frac{d^D p}{i(2\pi)^D} \left[\frac{1}{(p-k_2)^2 - m^{*2}} \frac{1}{p^2 - m^{*2}} \frac{1}{(p+k_1)^2 - m^{*2}} \right], \tag{87}$$

where e is the QED coupling constant and k_1 and k_2 are the external momentum of emitted photons so the square of the total momentum coincides with that of the original pion, namely, $(k_1 + k_2)^2 = m_\pi^2$. By using T_γ, the decay width, $\Gamma_{\pi^0 \gamma\gamma}$, is expressed as

$$\Gamma_{\pi\gamma\gamma} = \frac{m_\pi^3}{64\pi} |T_\gamma|^2. \tag{88}$$

The detailed derivation is presented in the paper [27]. After some algebra, one obtains

$$T_\gamma = -4g_{\pi qq} \frac{\alpha_e N_c m^*}{3\pi} \frac{(4\pi M_0^2)^{2-D/2}}{(m^{*2})^{3-D/2}} \frac{\Gamma(2-D/2)}{\hat{m}_\pi^2}$$

$$\times \int_0^1 dx \frac{1}{x} \left\{ \left[1 - x(1-x)\hat{m}_\pi^2 \right]^{-2+D/2} - 1 \right\} \tag{89}$$

with $\alpha_e = e^2/(4\pi)$, and $\hat{m}_\pi^2 = m_\pi^2/m^{*2}$.

With the observables, $m_\pi = 135$ MeV, $f_\pi = 94$ MeV and

$$\Gamma_{\pi^0 \gamma\gamma} = 7.8 \text{ eV}, \tag{90}$$

we perform the parameter fitting in the DR following [27]. Table 5 shows the fitted parameters in the DR case. We note that both the constituent quark mass and chiral condensate grow up with increasing m_u, which is the characteristic feature in this regularization [37]. The values, $\langle \bar{u}u \rangle$, almost coincide with the other regularizations for the same m_u, since Eq. (85) is the regularization independent relation in the model.

5. Meson properties

We have presented the required equations in the model, then set the parameters for various regularizations. It is now ready for the actual numerical analysis on the model predictions. Here

we shall show the thermal meson properties, which are the pion mass, the pion decay constant, and the sigma meson mass.

At finite temperature, there are two ways of the application of each regularization; one is to apply the regularization only for the temperature independent contribution because the temperature dependent contributions are always finite due to the characteristic factor of the Fermi–Dirac distribution, i.e., $f(E)$. The other is to apply the regularization both for the temperature independent and dependent parts, since the regularization essentially relates to the cutoff of the model so the introduction of the same cutoff clearly determines the model scale. On the other hand, the former method retains more symmetry of the model. Then the physical meanings of these prescriptions are that the former one respects the model symmetry, and the latter does the cutoff scale of the model. Since the model is not renormalizable, the predictions depend on the regularization ways and our purpose in this paper is to study the regularization dependence on the model. Therefore we shall study all the cases and compare the results among various regularizations.

5.1. Results with regularizing T-independent contribution

In this subsection, we show the results of meson properties based on the procedure of applying the regularization only to the temperature independent part. The required integrals are $\mathrm{tr}S$ and $I(p^2)$, and we evaluate the following combination,

$$\mathrm{tr}S = \mathrm{tr}S_{\mathrm{Reg}}^0 + \mathrm{tr}S^T \tag{91}$$

where $\mathrm{tr}S_{\mathrm{Reg}}^0$ is $\mathrm{tr}S$ for $T = 0$. The lower index indicates each regularization, namely, $\mathrm{tr}S_{\mathrm{3D}}^0$, $\mathrm{tr}S_{\mathrm{4D}}^0$, $\mathrm{tr}S_{\mathrm{PV}}^0$, $\mathrm{tr}S_{\mathrm{PT}}^0$ and $\mathrm{tr}S_{\mathrm{DR}}^0$. For the temperature dependent part $\mathrm{tr}S^T$, here we use the form shown in Eq. (24). Similarly for $I(p^2)$, we use the equivalent expression,

$$I(p^2) = I_{\mathrm{Reg}}^0(p^2) + I^T(p^2), \tag{92}$$

with I_{Reg}^0 for each regularization way.

Fig. 2 shows how the pion mass changes with respect to T and μ for various parameter sets in the previous section. It should be noted that, for some parameter sets, no real solution exists at high temperature as seen in the case with the DR and $m_u = 3.0$ MeV [31]. We observe the similar behavior in each regularization; the pion mass remains almost constant for low T and μ, then raises up for higher T and μ. This comes from the fact that the chiral symmetry is broken at low T and μ and restores at high T and μ. The pion has smaller mass when the symmetry is broken due to the Nambu–Goldstone theorem, while the mass becomes large after symmetry restoration. We see that the mass starts to increase around 170 MeV which is comparable to the critical temperature for the chiral symmetry breaking. We see that the temperature and chemical potential where the pion mass glows up become larger with respect to m_u for the 3D cutoff, 4D cutoff, PV and PT, while they become smaller for the DR. We also see that the discontinuity seen around the transition temperature is considerably larger in the DR case compare to the other regularizations. Then we expect that the tendency of the first order phase transition is strong for the DR comparing the other regularizations. We will discuss the issue in more detail in the next section.

The results of the pion decay constant are shown in Fig. 3. One sees the similar tendency as well; the decay constant is almost constant for low T and μ, and it decreases when T and μ exceed certain values which are around $T \simeq 170$ MeV and $\mu \simeq 300$–400 MeV. It is interesting to
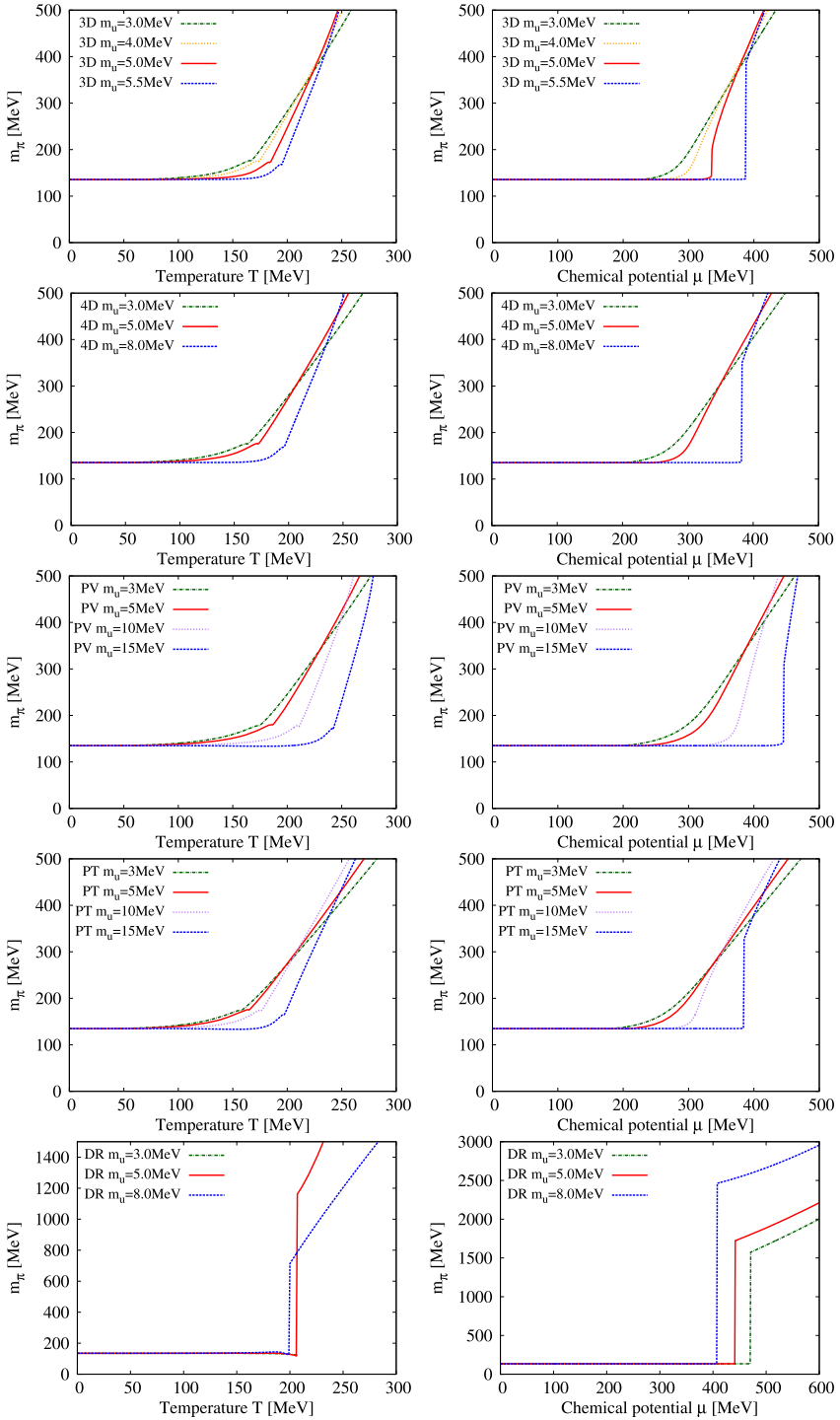
Fig. 2. Pion mass. Left: $\mu = 0$. Right: $T = 0$.
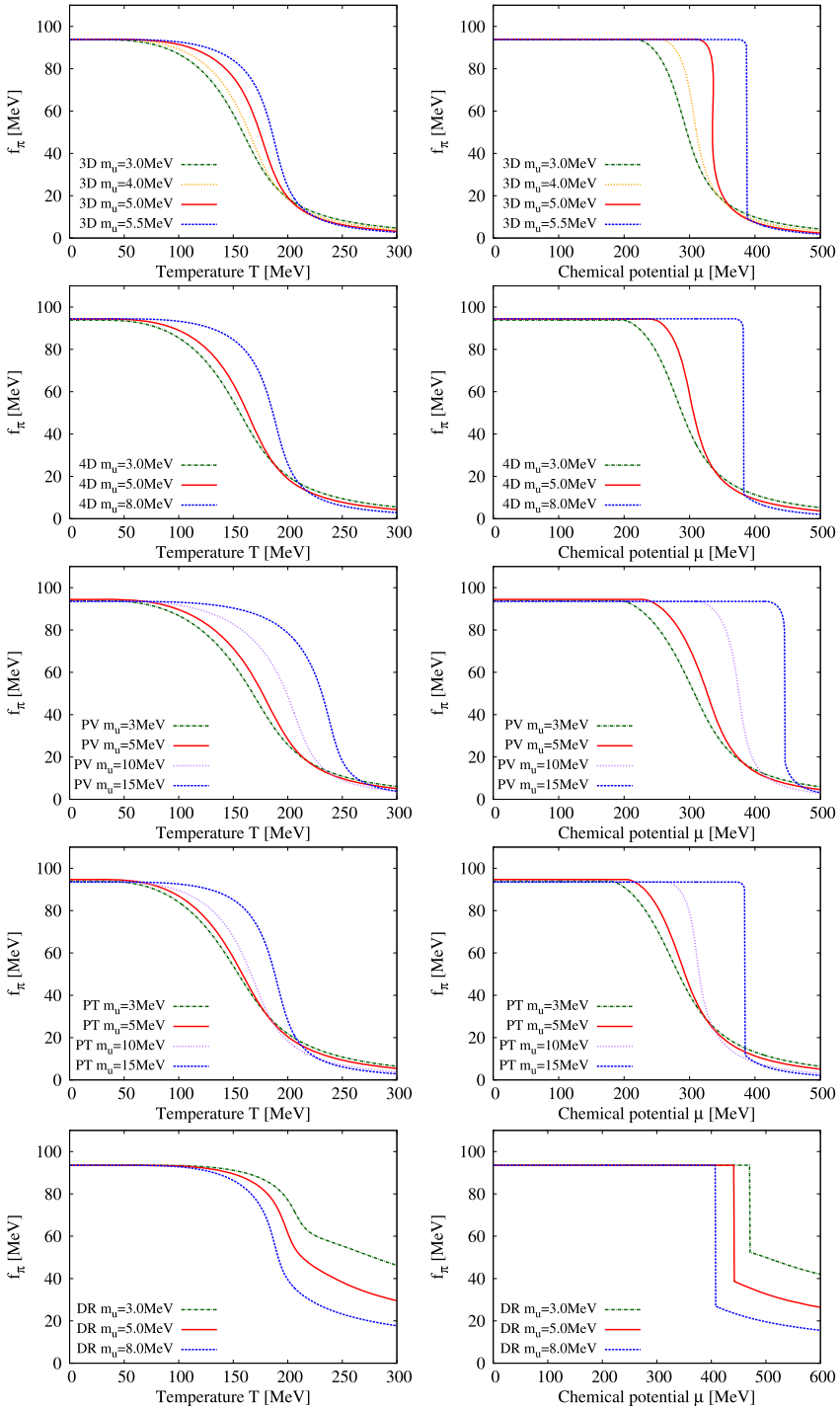
Fig. 3. Pion decay constant. Left: $\mu = 0$. Right: $T = 0$.

note that the decay constant drops discontinuously at high μ for some parameter sets in the 3D, 4D, PV, PT regularizations, while the discontinuity is always the case in the DR. The existence of the gap is the signal of the first order phase transition, and the tendency becomes stronger with increasing m_u. This is because the coupling strength is larger for higher m_u as seen from the parameter tables, so quarks have stronger correlations when the parameter m_u is larger in the 3D, 4D, PV, PT cases.

Having fixed the parameters with the pion mass and decay constant, we will calculate the sigma meson mass. It is one of the predictions of the model. Fig. 4 shows the numerical results of the sigma meson mass. At $T = 0$ and $\mu = 0$ we find the band around 400–900 MeV in 3D, 4D, PV, PT regularizations, 900–1400 MeV in the DR. It is known that the sigma meson mass is slightly higher than $2|m^*|$ [7]. Then, in the DR case, the predicted values are larger than the experimental value $m_\sigma = 400$–550 MeV, in the leading order of the $1/N_c$ expansion. As is known we can obtain much smaller sigma meson width in this order. We should also check the next to leading order contributions for the sigma meson mass and width [41]. The features of the curves are the similar to that of the pion; the mass decreases with increasing T and μ until some values, then it increases after exceeding the certain values. As seen in the pion mass case, the solution of the sigma mass on the real axis disappears for some parameter set at high temperature.

5.2. Results with regularizing all contribution

In this subsection, we study the meson properties by applying each regularization procedure to both temperature dependent and independent contributions. Here we will use the abbreviated expression, RT, to indicate the results with "regularizing also temperature dependent part". It is worth mentioning that the case with 4D cutoff method does not give credible results because enough number of frequency summations is not taken in this method. The cutoff scale of the 4D case is around 1 GeV, which means that at $T = 100$ MeV only four terms in the Matsubara mode summation, $n = -2, \pm 1, 0$ ($\omega_n = (2n + 1)\pi T$), are taken into account. It is known that finite temperature field theory does not lead reliable predictions when the number of the frequency summation is small [43]. Therefore, we will not show the results in the case of 4D cutoff scheme here, and consider the other four cases 3D, PV, PT and DR and call these cases 3DRT, PVRT, PTRT and DRRT, respectively. It is also worth mentioning that the calculations technically become impossible at $T = 0$ in the PTRT case as can be read from Eqs. (67) and (72). Then, we will show the results with $T = 10$ MeV as the representative values on μ dependence at low T.

Fig. 5 displays the results of the pion mass. One sees that the qualitative feature does not change comparing to the previous case with regularizing only the temperature independent contributions. Quantitatively, we note that the changes become smoother at high T and μ. This can easily be understood because the regularization procedure suppresses the thermal contribution, so the finite temperature term reduces to give smoother curve with respect to T and μ.

We aligned the results of the pion decay constant in Fig. 6. As seen in the pion mass case, the numerical results do not alter qualitatively, the curves become smooth. Note that, although the T dependence becomes considerably smother, the transition chemical potential does not change. This is due to the fact that finite temperature contributions become proportional to the step function $\theta(\mu - m^*)$ for $T = 0$, then the transition chemical potential is not affected by the regularization procedure in this model treatment.
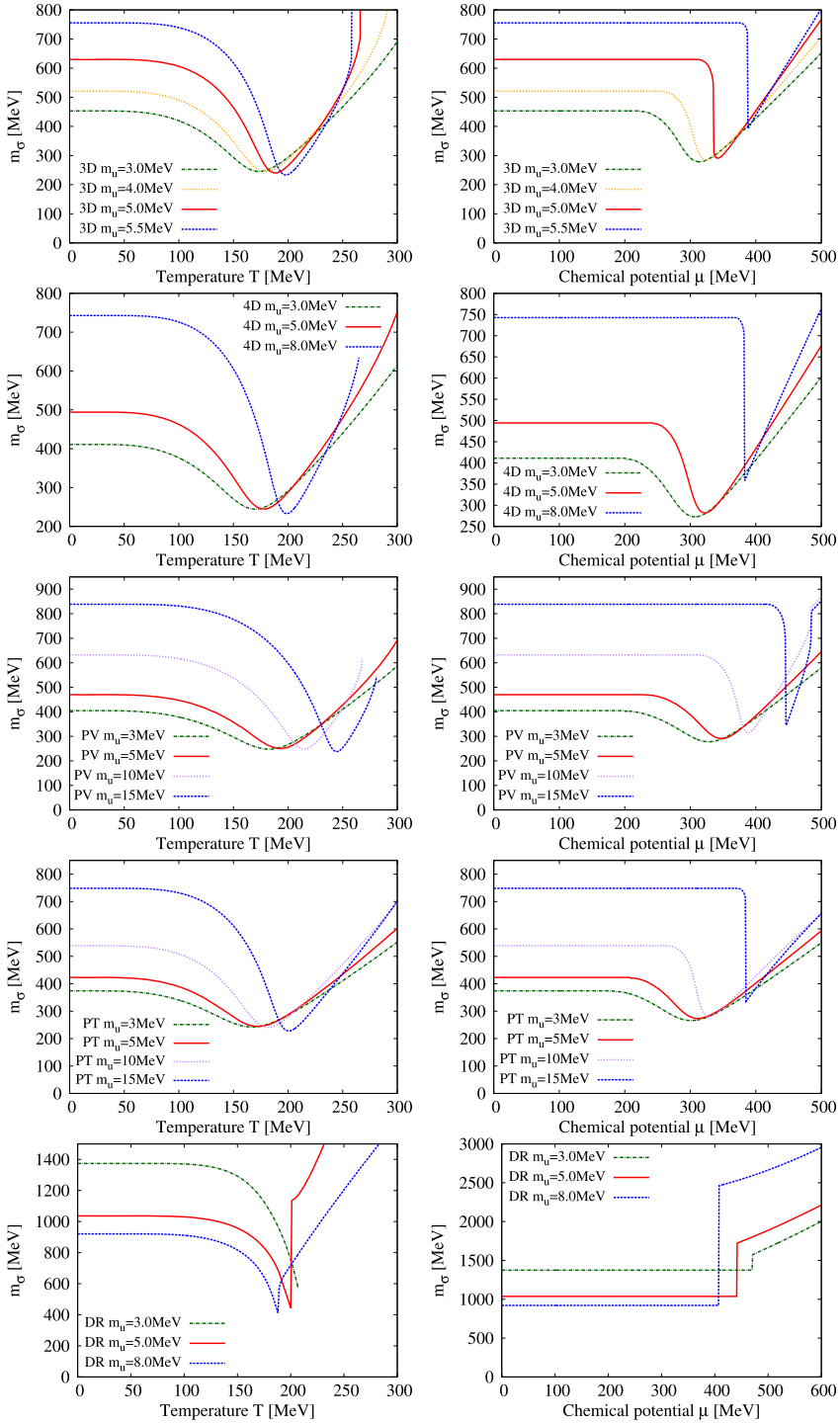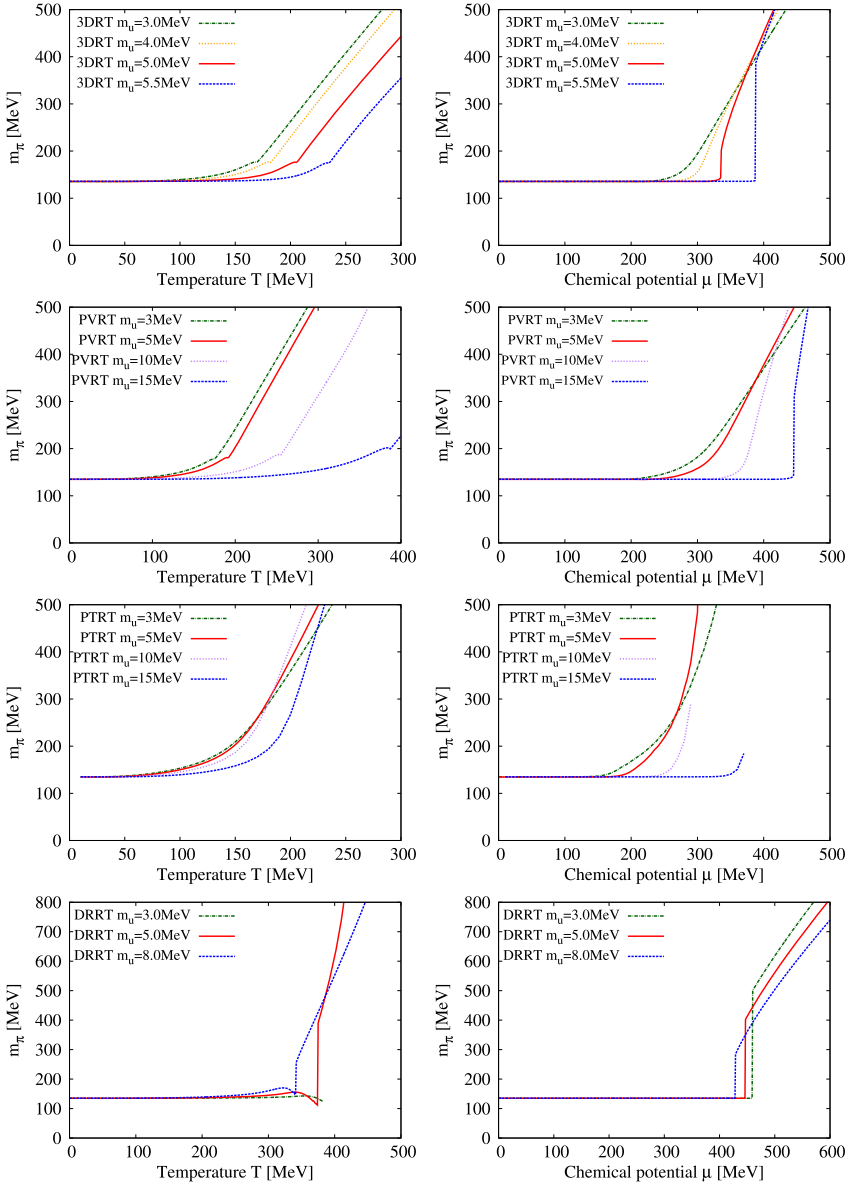
Fig. 4. Sigma mass. Left: $\mu = 0$. Right: $T = 0$.

Fig. 5. Pion mass. Left: $\mu = 0$. Right: $T = 0$ for 3DRT, PVRT, DRRT and $T = 10$ MeV for PTRT.

The predictions on the sigma meson mass are shown in Fig. 7. The deviations from the results in the previous subsection in Fig. 4 are more or less similar to the deviations on the pion mass; the curves become flatter with respect to T while μ dependence does not indicate much difference for the 3D, PV and PT cases. However, there appears substantial difference between the cases of the DR and DRRT where the values of the sigma meson mass at $\mu = 500$ MeV are around 1500–2500 MeV for the DR and around 600 MeV for the DRRT case. This comes from the
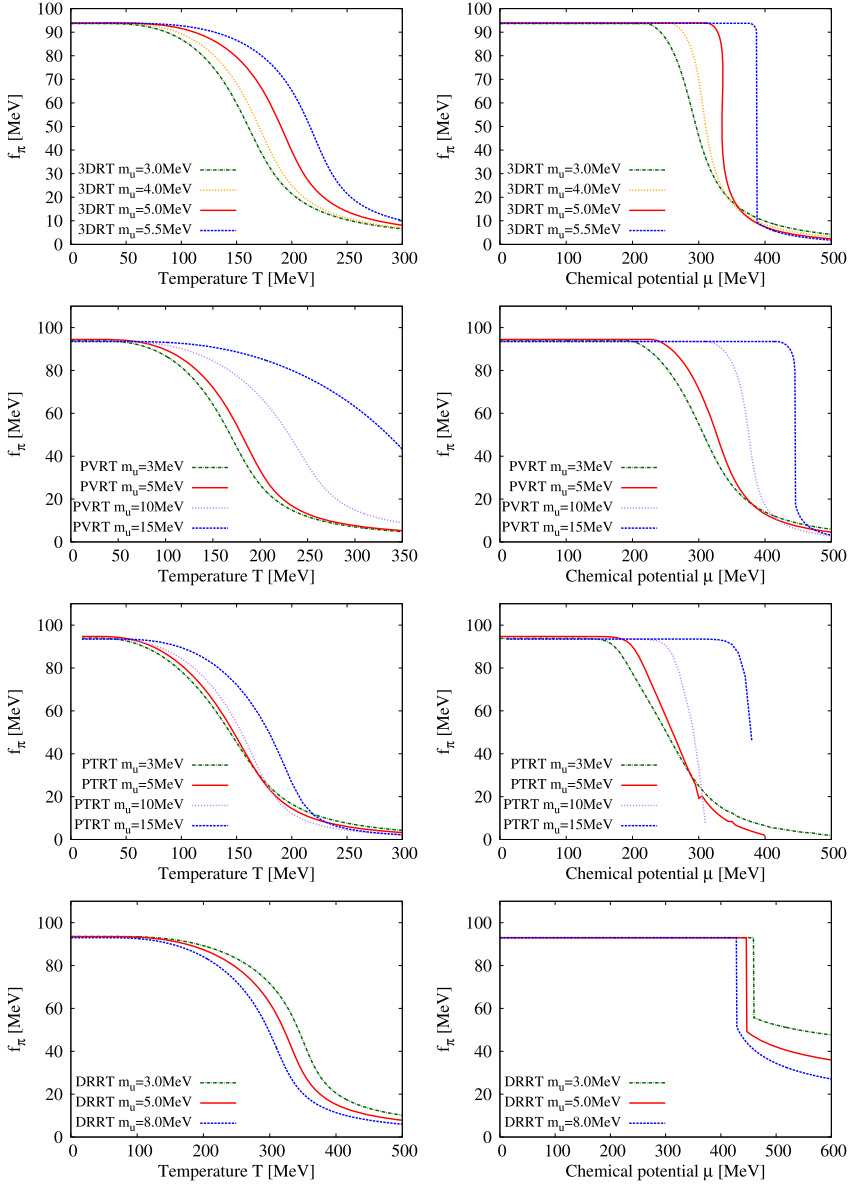
Fig. 6. Pion decay constant. Left: $\mu = 0$. Right: $T = 0$ for 3DRT, PVRT, DRRT and $T = 10$ MeV for PTRT.

difference of the integral values between these two cases, which we will discuss in more detail in Section 9.

We find that the solution on the real axis always disappears for high μ and low T (=10 MeV) in the PTRT with $m_u = 10$, 15 MeV. This is because for high μ some quantities become pure imaginary number in the calculation due to the complicated counter integral of $I_{\mathrm{PT}}(p^2)$ as seen
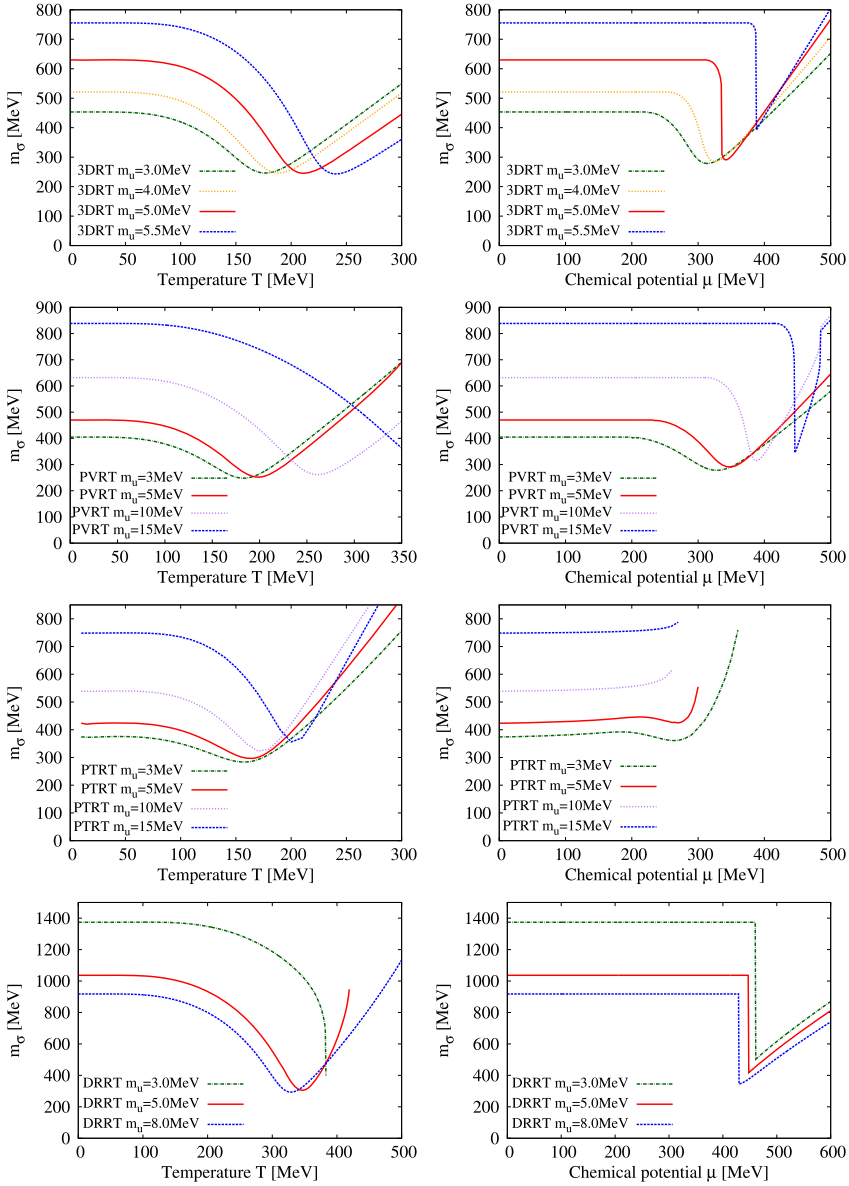
Fig. 7. Sigma mass. Left: $\mu = 0$. Right: $T = 0$ for 3DRT, PVRT, DRRT and $T = 10$ MeV for PTRT.

in Eq. (72). Then one cannot find a real solution in that case. This is the numerical reason why the meson properties behave badly for high μ in PTRT case.

6. Phase diagram

We shall draw the phase diagram in this section. We search the phase transition point by the condition that the maximum change of the chiral condensate with respect to T and μ. In more

concrete, we numerically differentiate the condensate with respect to $r \equiv \sqrt{T^2 + \mu^2}$, then the condition can be written

$$\frac{d\langle \bar{u}u \rangle^{1/3}}{dr} \bigg|_{T=T_c, \mu=\mu_c} = \text{Max} \left(\frac{d\langle \bar{u}u \rangle^{1/3}}{dr} \right). \tag{93}$$

We should be careful on the case with the first order transition, because the condensate has the discontinuous point where we need to find the minimum of the thermodynamic potential then determine the chiral condensate. No matter whether the phase transition is the first order or cross over, we can also use the above criterion since at the first order point, $d\langle \bar{u}u \rangle^{1/3}/dr = \infty$ holds, therefore it is consistent in both cases.

By searching the maximum number of the differentiate of the chiral condensate following the condition Eq. (93), we draw a phase boundary for the chiral symmetry. Fig. 8 shows the phase diagrams for the various parameter sets with fixed m_u ($\langle \bar{u}u \rangle$) and regularizations. One sees that the critical temperatures, T_c is found between 150 and 250 MeV at $\mu = 0$ if we regularize only the temperature independent parts (left four panels and the bottom panel). On the other hand, a higher critical temperature is observed when the regularization is applied to the temperature dependent and independent parts. The regularizations 3DRT and PTRT give a critical temperature around $T_c \simeq 200$ MeV at $\mu = 0$, the PVRT induces a higher critical temperature near $T_c \simeq 400$ MeV with $m_u = 15$ MeV, and the DRRT indicates it around $T_c = 300$–400 MeV. One also sees that the critical chemical potential, μ_c, has no large dependence on the application of the regularization to finite temperature term, because the terms are dominated by the step function $\theta(\mu - m^*)$ as mentioned in the previous section. Consequently, the area of phase boundary enlarges in the T direction when we apply the regularization to the temperature dependent term, which is numerically confirmed by the figure.

The phase boundary resembles each other for $m_u = 3.0$ and 5.0 MeV cases in 3D, 4D, PV and PT, especially in small μ region. However for $m_u = 15$ MeV, the phase boundary in PV is far from the one in PT. These results show that the regularization dependence for the phase boundary become large as decreasing the cutoff scale. Comparing the result for 3D, PV, PT, DR with that for 3DRT, PVRT, PTRT, DRRT, we find that the chiral symmetry breaking phase enlarges in the small μ region. This tendency becomes stronger as decreasing the cutoff scale.

We think the most interesting comparison from the figure is on the existence of the critical end point where the first order phase transition starts on the phase boundary. For 3D, 4D, PV, PT, no critical end point appears for the parameter sets with small m_u. While the critical end point always appears in DR. Then we can numerically conclude that the DR has stronger tendency of the first order phase transition comparing with the other regularizations. The existence of the critical end point in the other four regularizations can be understood by seeing the value of the parameter G. Briefly speaking, the critical end point appears when G is large. This is physically reasonable because G represents the strength of the correlation between quarks, then the larger G makes the condensation stronger.

7. Phase diagram with fixing $|m^*|$

We have seen the phase diagram and how the location of the critical end point depends on the parameters in the various regularizations. Considering the fact that the transition T and μ is essentially determined by the value of the constituent quark mass since its dependence appears in the thermal distribution, $f(E)$, with $E = \sqrt{k^2 + m^{*2}}$, we think it may as well be interest-
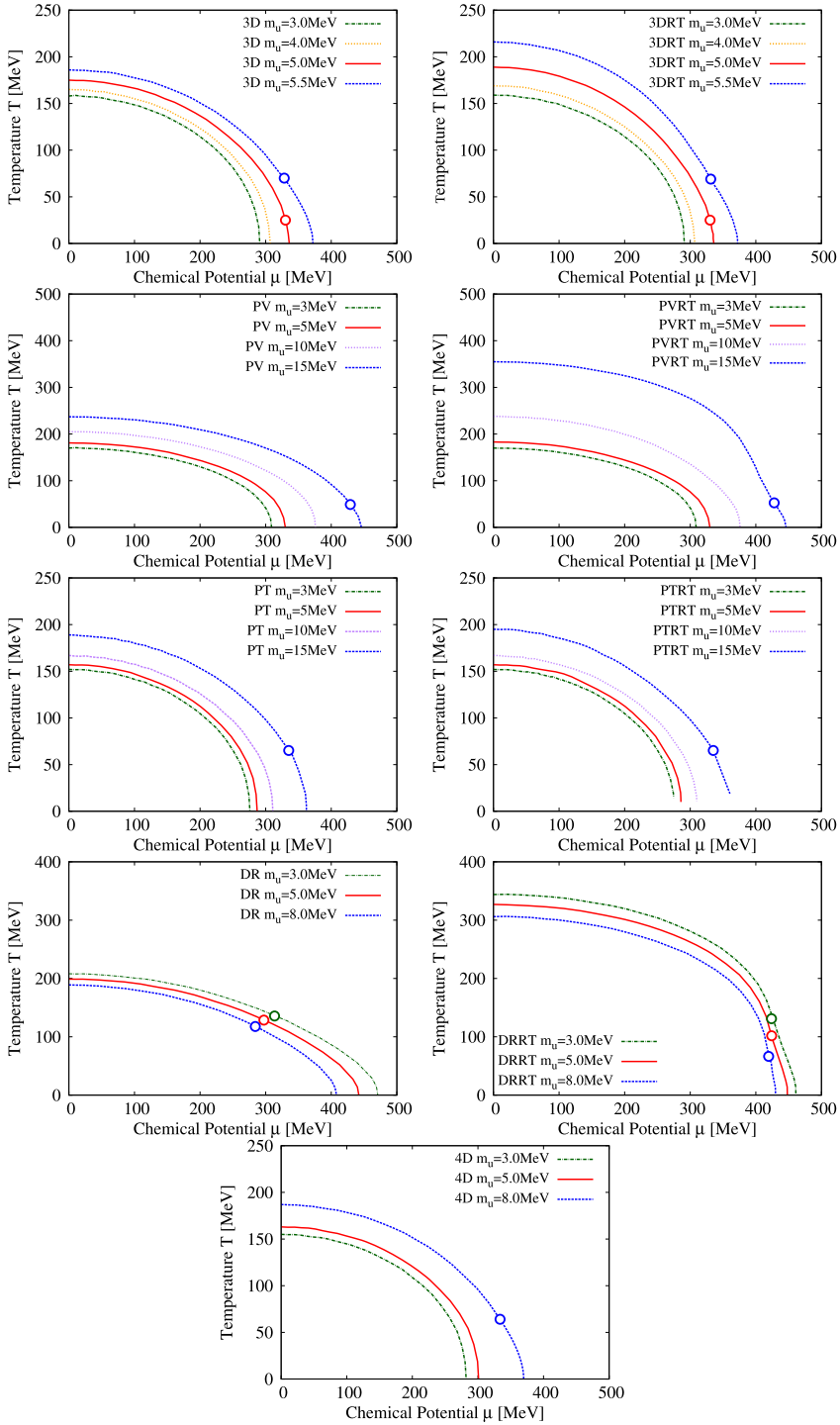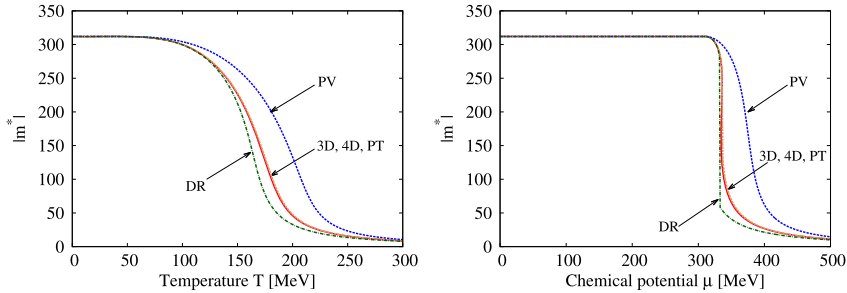
Fig. 8. Phase diagram.

Table 6
Parameters fixed with $|m^*| = 311$ MeV.

	m_u (MeV)	Λ (MeV)	D	G (MeV^{-2})	M_0 (MeV)	$\langle \bar{u}u \rangle^{1/3}$ (MeV)
3D	5.0	665	(4)	4.71×10^{-6}	–	−253
4D	7.1	827	(4)	6.66×10^{-6}	–	−225
PV	9.94	780	(4)	9.56×10^{-6}	–	−199
PT	12.6	680	(4)	12.1×10^{-6}	–	−183
DR	20.9	–	3.32	-2.29×10^{-4}	37	−160

Fig. 9. Comparison of the constituent quark mass with fixed parameters under $|m^*| = 311$ MeV. Left: $\mu = 0$. Right: $T = 0$.

ing to compare the phase diagram with the parameter sets which lead the same value of $|m^*|$ (=311 MeV) at $T = 0$ and $\mu = 0$ instead of fixing the current quark mass, m_u.

In Table 6, we align the parameters for each regularization methods. One more parameter is necessary for the DR case. Note that G means GM_0^{4-D} in DR. We see that the value of the current quark mass which leads $|m^*| = 311$ MeV is close to the one in Ref. [38] for the 3D case, while the other regularizations give relatively larger values.

Having fixed the parameters, we are now ready to show the phase diagram based on the one with regularizing only the temperature independent parts, 3D, 4D, PV, PT and DR. The behaviors of m^* for each regularization are shown in Fig. 9. All the results have no large difference, because the gap equations of the temperature independent part for each regularization has the similar behavior. The gap equations contain the following form,

$$\text{tr} S^0(m^*) \ni f(m^*, \Lambda) + m^{*2} \ln(g(m^*, \Lambda)), \tag{94}$$

in the regularizations, 3D, 4D, PV and PT. While in the DR, m^* and Λ are replaced by M_0 and D in some parts (see Appendix B). In Fig. 9, we note that the results almost coincide in three regularizations, 3D, 4D and PT. The behavior in PV shows a smaller and DR gives steeper slope than the others.

In Fig. 10 the phase diagram is illustrated in each regularization. The phase boundaries of 3D, 4D and PT show almost equivalent behavior. The area of the chiral symmetry broken phase for PV is larger than the others. This tendency comes from the behavior of m^* in Fig. 9. Since Λ_{PV} is entered in the form of the dynamical mass, the chiral symmetry breaking contribution is enhanced than the other regularizations. The area for the chiral symmetry broken phase for the DR is smaller than the others. The critical end point for the DR locates at higher temperature than the one for 3D, 4D and PT. These tendency also comes from the behavior of m^* in Fig. 9.
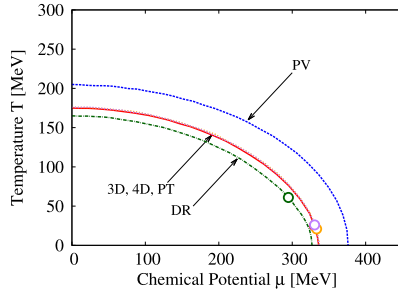
Fig. 10. Comparison of the phase diagrams with fixed parameters under $|m^*| = 311$ MeV.
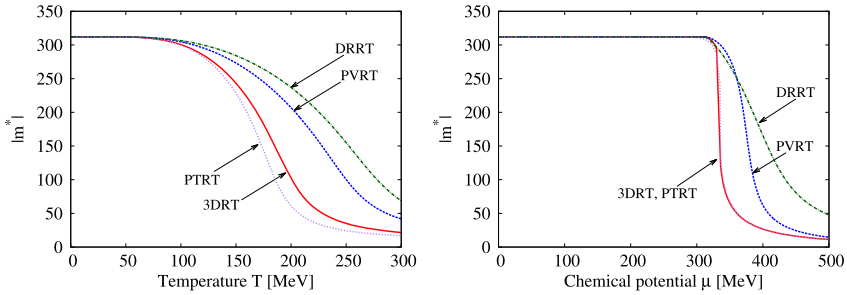
Fig. 11. Comparison of the constituent quark mass with fixed parameters under $|m^*| = 311$ MeV. Left: $\mu = 0$. Right: $T = 0$ for 3DRT, PVRT, DRRT and $T = 10$ MeV for PTRT.
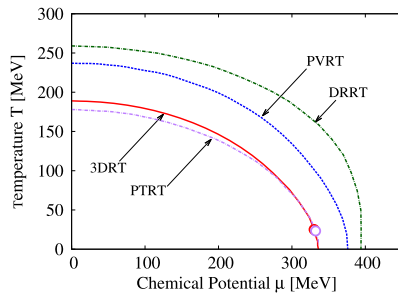
Fig. 12. Comparison of the phase diagrams with fixed parameters under $|m^*| = 311$ MeV.

Next, we discuss the results with regularizing both the temperature independent and dependent parts, 3DRT, PVRT, PTRT and DRRT. The behavior of m^* for each regularization is shown in Fig. 11. We find that the finite temperature effect becomes smaller or softer than 3D, PV, PT and DR, respectively. The behavior of m^* in DRRT is the closest to the case of its regularizing only temperature independent part.

The chemical potential has the similar contribution for 3DRT, PTRT, and PVRT. The behaviors of m^* in DRRT and DR have large difference. This difference is caused by the reduction of the momentum integral dimension, D, from 4 to 3.32.

The phase diagram in each regularization is shown in Fig. 12. To compare with Fig. 10, the region of the broken phase enlarges in PTRT, 3DRT and PVRT for a low chemical potential. However, the critical chemical potentials in PTRT, 3DRT and PVRT for a low temperature are

Table 7
Critical end point for each regularization.

Regularization	μ_{CP} (MeV)	T_{CP} (MeV)
3D	330	25.0
4D	333	46.8
PT	330	26.0
DR	289	74.7
3DRT	330	25.0
PTRT	332	23.2

Table 8
Parameters fixed with $T_c = 175$ MeV.

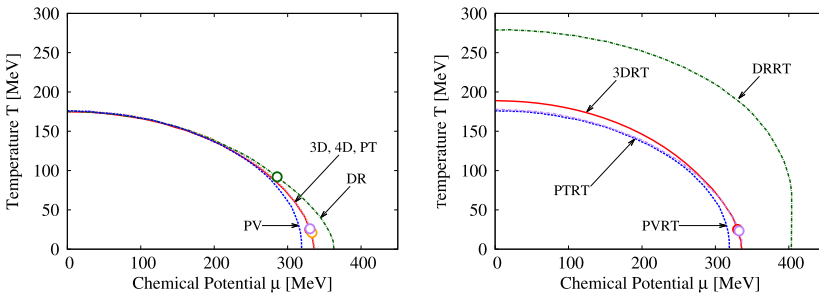|	m_u (MeV)	Λ (MeV)	D	G (MeV^{-2})	M_0 (MeV)	m^* (MeV)	$\langle \bar{u}u \rangle^{1/3}$ (MeV)
3D	5.0	665	(4)	4.71×10^{-6}	–	311	−253
4D	7.1	827	(4)	6.66×10^{-6}	–	311	−225
PV	4.0	1209	(4)	2.56×10^{-6}	–	212	−272
PT	12.6	680	(4)	12.1×10^{-6}	–	311	−183
DR	14.0	–	3.10	-6.09×10^{-4}	56	−375	−181

Fig. 13. Comparison of the phase diagrams with the parameters in Table 8.

almost equivalent to that in PT, 3D and PV, respectively. From the behavior of m^* in Fig. 11, we observe a larger critical temperature and chemical potential for DRRT. We display the location of the critical end points (μ_{CP}, T_{CP}) for each regularization in Table 7.

8. Phase diagram with fixing T_c

We have shown the phase structure with fixing the value of the constituent quark mass at $T = 0$ and $\mu = 0$ for each regularization method in the previous section. It is also interesting to study the case with the parameters which lead the equal transition temperature for $\mu = 0$. The explicit parameters fixed with the condition $T_c = 175$ MeV for $\mu = 0$ are shown in Table 8.

Let us show the phase diagrams for various regularizations. The left panel of Fig. 13 displays the phase diagram with the parameters given in Table 8. We see the same critical temperature for $\mu = 0$ which is due to the parameter setting, and the curves deviate for low T and high μ. The phase diagrams in the 3D, 4D and PT cases become almost equivalent. On the other hand the critical chemical potential for low T in the PV (DR) is smaller (larger) than the other three cases. The difference comes from the different values of the constituent mass m^* at $T = 0$ and

$\mu = 0$ where $m^* = 311$ MeV in the 3D, 4D, PT, 212 MeV in the PV and -375 MeV in the DR. The characteristic difference is that the critical end point in the DR case locates at higher temperature, $(\mu_{CP}, T_{CP}) = (285$ MeV, 92 MeV$)$, than the other regularizations as observed in Fig. 10. Therefore we can say that the DR has stronger tendency of the first order phase transition than the other regularizations.

The effect of regularizing the temperature dependent part on the phase diagram is shown in the right panel of Fig. 13. One sees that the cases 3DRT, PVRT and PTRT exhibit the similar diagrams with the 3D, PV, and PT cases, respectively. While the DRRT shows the larger area for the broken phase on T–μ plane as already seen in the difference between Figs. 10 and 12. The difference comes from the nature of the regularization of treating integral region, which we will give detailed discussion in the next section.

9. Discussions

We have introduced the regularization methods then studied the meson properties and phase diagram in previous sections. In this section, we are going to present more detailed discussions on the obtained results.

In comparing the left panels vs. right panels in Fig. 8, one can observe the contribution to apply the regularization procedure to the thermal correction. The phase diagram does not show considerable difference for 3D and PT cases, while in PV the area of the phase boundary becomes larger in the right panel when m_u is large, and the areas in DRRT case is larger than DR case for all the parameter sets. This difference can be understood through the following discussion.

The loop integral, $\mathcal{I}$, essentially has the following subtracted forms for 3DRT, PVRT, and PTRT,

$$\mathcal{I}_{3DRT} = \int_0^\infty d^3k \, F(k) - \int_\Lambda^\infty d^3k \, F(k), \tag{95}$$

$$\mathcal{I}_{PVRT} = \int_0^\infty d^3k \left[F(k, m^*) - F(k, \Lambda) \right], \tag{96}$$

$$\mathcal{I}_{PTRT} = \int_0^\infty d^3k \left[F(k) - F(k)(1 - e^{-(k^2 + m^{*2})/\Lambda^2}) \right]. \tag{97}$$

Where the typical form of $F(k, m^*)$ is given by $F(k, m^*) = Cf(E)/E$ with some constant value, C. Thus the subtracted terms basically relate to the suppression on the high energy contributions which are expected to be small. We numerically confirmed that the subtracted parts are small for almost all the cases, then the phase diagram does not change drastically. However, in the PV case with large m_u, the difference between $F(k, m^*)$ and $F(k, \Lambda)$ is small since the constituent quark mass becomes comparable to the cutoff scale, e.g., $m^* = 417$ MeV and $\Lambda_{PV} = 729$ MeV for $m_u = 15$ MeV in PV. Consequently, the thermal contribution strongly suppressed in the PV case with large m_u.

We saw that the area of the phase boundary does not alter so much in 3D, PV and PT regularizations. The essential reason is that the infinities appearing from loop integrals are subtracted at high energy. However in DR, the situation is different since the integral is replaced as

$$\int_0^\infty \mathrm{d}^4k \; F(k) \to \int_0^\infty \mathrm{d}^Dk \; F(k),\tag{98}$$

so this modifies the integral kernel rather than the subtraction of high energy modes. This is the reason why DR shows considerable difference, if we apply the regularization to both temperature independent and dependent contributions.

We also saw the location (or existence) of the critical end point is non-trivial. In Fig. 10, the diagram has the critical end point for 3D, 4D, PT and DR. No critical end point appears in the PV. Thus we find that the PV has weaker tendency of the first order phase transition than that of the other regularization methods. Particularly, the temperature of the critical end point in the DR case is higher than others, which may enable us to conclude that the DR has the stronger tendency of the first order phase transition.

10. Concluding remarks

We have studied the regularization dependence on the phase diagram of quark matter on $T-\mu$ plane by using the NJL model. We have first presented the regularization procedure at finite temperature and chemical potential, then fitted parameters within various regularization methods. Thereafter, we have studied the meson properties and the phase structure.

We find that the model produces the reliable predictions on the meson properties whose behavior for finite temperature and chemical potential well reflects the chiral symmetry breaking/restoring, which indicates that all the regularizations employed in this paper nicely capture physics on the meson properties. We can conclude that the regularizations are almost safely adopted. In this context the regularization parameter independent approach is also interesting [41,44].

The phase boundary is similar for small current quark mass cases, $m_u = 3.0$ and 5.0 MeV in 3D, 4D, PV and PT. As increasing (decreasing) the quark mass (cutoff scale), the regularization dependence for the phase boundary becomes larger. Comparing the results of 3D, PV and PT case with these of RT case, the chiral symmetry broken phase for RT case in the small μ region becomes larger as m_u increases.

We summarize the feature of the each regularization on the phase diagram. 1) The 3D case gives reasonable result with the most appropriate parameter set. Concerning on the phase boundary in the 3DRT case, the temperature part may not have enough contribution for small μ region as seen in Figs. 12 and 13. 2) The 4D case is almost the same with the 3D case as seen in Figs. 10 and 13. However RT case for 4D is ill defined. 3) PV and PVRT cases with small m_u are similar to the 3D case as shown in Fig. 13. It is to be noted that the first order phase transition does not appear in these cases. Then we confirm that the PV has weaker tendency of the first order transition. 4) PT and PTRT cases are almost the same with the 3D case in Fig. 13. Here, we should note that these cases are obtained by using the parameters with large value of m_u, such as 12.6 MeV. 5) The DR case with large m_u is adequate as seen in Figs. 10 and 13. It is interesting that the CP locates smaller μ and higher T comparing to the result in the other regularizations. The DRRT case cannot lead reliable results in our way of fixing the parameters. However, it may be worth mentioning that the DRRT case shows reasonable result with another parameter set obtained by the following inputs: pions mass, pion decay constant, current quark mass and critical temperature at $\mu = 0$ [34].

It is expected that observation of the critical end point can distinguish a suitable regularization for an effective model of QCD by comparing with the resulting phase diagrams. The important

difference is the existence of the critical end point. The model predicts that the critical end point appears at intermediate chemical potential around $\mu \simeq 300$–400 MeV. This density coincides with the one in which different quark state such as color superconductivity may occur, there the order of the phase transition might affect crucially on such the dense states. Moreover the color superconductivity may be realized in the dense stellar objects, like quark stars and neutron stars [34]. Therefore the study of the order of the phase transition has important meaning as well in cosmological observations. So we believe that the further and more extensive investigations are necessary on this subject.

Acknowledgements

Appendix A. Analytic expressions for $I^0(p^2)$

Since the $I^0(p^2)$ integral can be evaluated analytically, we will present the explicit expression for various regularizations.

One needs special care in performing $I(p^2)$ integral since it contains divergent contribution as seen in the 3D cutoff scheme. I^0_{4D} becomes for $m^{*2} > p^2/4$,

$$I^0_{4D}(p^2) = \frac{N_c}{4\pi^2}\left[\ln \frac{\Lambda^2_{4D} + m^{*2}}{m^{*2}} + 4a \arctan\left(\frac{1}{2a}\right) \right.$$
$$\left. - 4b \arctan\left(\frac{1}{2b}\right) - \frac{2\Lambda^2_{4D}}{ap^2}\arctan\left(\frac{1}{2a}\right) \right], \tag{A.1}$$

and for $m^{*2} < p^2/4$,

$$I^0_{4D}(p^2) = \frac{N_c}{4\pi^2}\left[\ln \frac{\Lambda^2_{4D} + m^{*2}}{p^2} + 4a \arctan\left(\frac{1}{2a}\right) \right.$$
$$\left. - 2\sum_{\pm}\left(\frac{1}{2}\pm b\right)\ln\left(\left|\frac{1}{2}\pm b\right|\right) - \frac{2\Lambda^2_{4D}}{ap^2}\arctan\left(\frac{1}{2a}\right) + 2i\pi b \right], \tag{A.2}$$

where

$$a = \sqrt{\frac{\Lambda^2_{4D} + m^{*2}}{p^2} - \frac{1}{4}}, \quad b = \sqrt{\left|\frac{\Lambda^2_{4D}}{p^2} - \frac{1}{4}\right|}. \tag{A.3}$$

Concerning on $I^0_{PV}(p^2)$, it is convenient that we divide the integral as

$$I^0_{PV} = I^{0(m)}_{PV} - I^{0(\Lambda)}_{PV}, \tag{A.4}$$

where $I^{0(\Lambda_{PV})}_{PV}$ is subtracted part in the original integral and it becomes

$$I^{0(\Lambda)}_{PV} = -\frac{N_c}{2\pi^2}\sum_{\pm}\left[\left(\frac{1}{2}\pm c\right)\ln\left(\frac{1}{2}\pm c\right)\right], \tag{A.5}$$

with

$$c = \sqrt{\frac{(\Lambda_{\text{PV}}^2 - m^{*2} + p^2)^2}{4p^4} - \frac{\Lambda_{\text{PV}}^2}{p^2}}. \tag{A.6}$$

As seen above, we need to separately evaluate the integral $I_{\text{PV}}^{0(m)}$ depending on the values of m^{*2} and p^2. It becomes for $m^{*2} > p^2/4$,

$$I_{\text{PV}}^{0(m)} = -\frac{N_c}{4\pi^2}\left[-2 + \ln\left(m^{*2}\right) + 4d\arctan\left(\frac{1}{2d}\right)\right], \tag{A.7}$$

and for $m^{*2} < p^2/4$,

$$I_{\text{PV}}^{0(m)} = -\frac{N_c}{2\pi^2}\sum_{\pm}\left[-1 + \left(\frac{1}{2}\pm h\right)\ln\left(\left|\frac{1}{2}\pm h\right|\right) - i\pi h\right], \tag{A.8}$$

where

$$d = \sqrt{\frac{m^{*2}}{p^2} - \frac{1}{4}}, \quad h = \sqrt{\frac{1}{4} - \frac{m^{*2}}{p^2}}. \tag{A.9}$$

Appendix B. $\text{tr}S_{\text{DR}}^0$ and f_π for $D \simeq 2, 3, 4$

We arrange the concrete expressions for $\text{tr}S_{\text{DR}}^0$ and f_π.
For $D \simeq 2$, $(D = 2 + 2\epsilon)$ we have

$$\text{tr}S_{\text{DR}}^0 \simeq \frac{N_c}{2\pi^2}m^* \cdot M_0^2\left[\frac{1}{\epsilon} + \gamma_E - \ln(2\pi) + \ln\frac{m^{*2}}{M_0^2}\right], \tag{B.1}$$

$$f_{\pi\text{DR}}^2 \simeq \frac{N_c}{2\pi}M_0^2\left[1 + \epsilon\left\{\gamma_E - \ln(2\pi) + \ln\frac{m^{*2}}{M_0^2}\right\}\right]. \tag{B.2}$$

For $D \simeq 3$, $(D = 3 + 2\epsilon)$ we have

$$\text{tr}S_{\text{DR}}^0 \simeq \frac{N_c}{\sqrt{2}\pi}m^* \cdot \sqrt{m^{*2}}M_0\left[1 + \epsilon\left\{\gamma_E + \ln\frac{2}{\pi} - 2 + \ln\frac{m^{*2}}{M_0^2}\right\}\right], \tag{B.3}$$

$$f_{\pi\text{DR}}^2 \simeq \frac{N_c}{2\sqrt{2}\pi}\sqrt{m^{*2}}M_0\left[1 + \epsilon\left\{\gamma_E + \ln\frac{2}{\pi} + \ln\frac{m^{*2}}{M_0^2}\right\}\right]. \tag{B.4}$$

For $D \simeq 4$, $(D = 4 - 2\epsilon)$ we have

$$\text{tr}S_{\text{DR}}^0 \simeq \frac{N_c}{4\pi^2}m^* \cdot m^{*2}\left[\frac{1}{\epsilon} - \gamma_E + \ln(2\pi) + 1 + \ln\frac{M_0^2}{m^{*2}}\right], \tag{B.5}$$

$$f_{\pi\text{DR}}^2 \simeq \frac{N_c}{4\pi^2}m^{*2}\left[\frac{1}{\epsilon} - \gamma_E + \ln(2\pi) + \ln\frac{M_0^2}{m^{*2}}\right]. \tag{B.6}$$

References

[1] M.A. Stephanov, Prog. Theor. Phys. Suppl. 153 (2004) 139;
    M.A. Stephanov, Int. J. Mod. Phys. A 20 (2005) 4387;
    M.A. Stephanov, PoS LAT 2006 (2006) 024;
    O. Philipsen, Prog. Theor. Phys. Suppl. 174 (2008) 206;
    W. Weise, Prog. Theor. Phys. Suppl. 186 (2010) 390;
    K. Fukushima, T. Hatsuda, Rep. Prog. Phys. 74 (2011) 014001;
    G. Endrodi, Z. Fodor, S.D. Katz, K.K. Szabo, J. High Energy Phys. 1104 (2011) 001.
[2] D. Gross, F. Wilczek, Phys. Rev. Lett. 30 (1973) 1343.
[3] K.G. Wilson, Phys. Rev. D 10 (1974) 2445.
[4] Y. Nambu, G. Jona-Lasinio, Phys. Rev. 122 (1961) 345;
    Y. Nambu, G. Jona-Lasinio, Phys. Rev. 124 (1961) 246.
[5] U. Vogl, W. Weise, Prog. Part. Nucl. Phys. 27 (1991) 195.
[6] S.P. Klevansky, Rev. Mod. Phys. 64 (1992) 649.
[7] T. Hatsuda, T. Kunihiro, Phys. Rep. 247 (1994) 221.
[8] M. Buballa, Phys. Rep. 407 (2005) 205.
[9] M. Huang, Int. J. Mod. Phys. E 14 (2005) 675.
[10] W. Pauli, F. Villars, Rev. Mod. Phys. 21 (1949) 434.
[11] C. Itzykson, J.B. Zuber, Quantum Field Theory, McGraw-Hill Inc. Press, 1980.
[12] T.P. Cheng, L.F. Li, Gauge Theory of Elementary Particle Physics, Oxford University Press, 1984.
[13] J.S. Schwinger, Phys. Rev. 82 (1951) 664.
[14] G. 't Hooft, M.J.G. Veltman, Nucl. Phys. B 44 (1972) 189.
[15] D. Kahana, M. Lavelle, Phys. Lett. B 298 (1993) 397.
[16] A.A. Osipov, H. Hansen, B. Hiller, Nucl. Phys. A 745 (2004) 81.
[17] J. Moreira, B. Hiller, A.A. Osipov, A.H. Blin, Int. J. Mod. Phys. A 27 (2012) 1250060.
[18] H. Suganuma, T. Tatsumi, Ann. Phys. 208 (1991) 470.
[19] K.G. Klimenko, Theor. Math. Phys. 89 (1992) 1161;
    K.G. Klimenko, Teor. Mat. Fiz. 89 (1991) 211.
[20] K.G. Klimenko, Z. Phys. C 54 (1992) 323.
[21] V.P. Gusynin, V.A. Miransky, I.A. Shovkovy, Phys. Rev. Lett. 73 (1994) 3499;
    V.P. Gusynin, V.A. Miransky, I.A. Shovkovy, Phys. Rev. Lett. 76 (1996) 1005 (Erratum).
[22] T. Inagaki, S.D. Odintsov, Y.I. Shil'nov, Int. J. Mod. Phys. A 14 (1999) 481.
[23] T. Inagaki, D. Kimura, T. Murata, Prog. Theor. Phys. Suppl. 153 (2004) 321.
[24] T. Inagaki, D. Kimura, T. Murata, Prog. Theor. Phys. 111 (2004) 371.
[25] T. Inagaki, D. Kimura, T. Murata, Int. J. Mod. Phys. A 20 (2005) 4995.
[26] Z.F. Cui, Y.L. Du, H.S. Zong, Int. J. Mod. Phys. Conf. Ser. 29 (2014) 1460232.
[27] S. Krewald, K. Nakayama, Ann. Phys. 216 (1992) 201.
[28] R.G. Jafarov, V.E. Rochev, Cent. Eur. J. Phys. 2 (2004) 367.
[29] R.G. Jafarov, V.E. Rochev, Russ. Phys. J. 49 (2006) 364;
    R.G. Jafarov, V.E. Rochev, Izv. Vuz. Fiz. 49 (2006) 20.
[30] T. Inagaki, D. Kimura, A. Kvinikhidze, Phys. Rev. D 77 (2008) 116004.
[31] T. Inagaki, D. Kimura, H. Kohyama, A. Kvinikhidze, Phys. Rev. D 85 (2012) 076002.
[32] T. Inagaki, D. Kimura, H. Kohyama, A. Kvinikhidze, Phys. Rev. D 86 (2012) 116013.
[33] S. Benic, D. Horvatic, J. Klaric, Phys. Rev. D 89 (2014) 054025.
[34] T. Fujihara, D. Kimura, T. Inagaki, A. Kvinikhidze, Phys. Rev. D 79 (2009) 096008.
[35] M. Asakawa, K. Yazaki, Nucl. Phys. A 504 (1989) 668.
[36] T. Inagaki, T. Kouno, T. Muta, Int. J. Mod. Phys. A 10 (1995) 2241.
[37] T. Inagaki, D. Kimura, H. Kohyama, A. Kvinikhidze, Phys. Rev. D 83 (2011) 034005.
[38] K.A. Olive, et al., Particle Data Group Collaboration, Chin. Phys. C 38 (2014) 090001.
[39] F. Sannino, J. Schechter, Phys. Rev. D 52 (1995) 96.
[40] M. Harada, F. Sannino, J. Schechter, Phys. Rev. D 54 (1996) 1991.
[41] T. Inagaki, D. Kimura, H. Kohyama, Int. J. Mod. Phys. A 29 (2014) 1450048.
[42] M. Gell-Mann, R.J. Oakes, B. Renner, Phys. Rev. 175 (1968) 2195.
[43] J.W. Chen, H. Kohyama, U. Raha, Phys. Rev. D 83 (2011) 094014.
[44] T. Inagaki, D. Kimura, H. Kohyama, A. Kvinikhidze, Int. J. Mod. Phys. A 28 (2013) 1350164.